https://doi.org/10.5194/tc-2023-88
Preprint. Discussion started: 27 June 2023

The Cryosphere
Discussions
Open Access

Triggers of the 2022 Larsen B multi-year landfast sea ice break-out and initial glacier response

Naomi E. Ochwat[1,2]*, Ted A. Scambos[1], Alison F. Banwell[1], Robert S. Anderson[2], Michelle L. Maclennan[3], Ghislain Picard[4], Julia A. Shates[5], Sebastian Marinsek[6], Liliana Margonari[6], Martin Truffer[7,8], and Erin C. Pettit[9]

[1]Earth Science Observation Center, Cooperative Institute for Research in Environmental Sciences, University of Colorado, Boulder, CO, USA

[2]Department of Geology, University of Colorado, Boulder, CO, USA,

[3]Department of Atmospheric and Oceanic Sciences, University of Colorado, Boulder, CO, USA,

[4]Univ. Grenoble Alpes, CNRS, Institut des Géosciences de l'Environnement (IGE), UMR 5001, Grenoble, France

[5]Department of Atmospheric and Oceanic Sciences, University of Wisconsin–Madison, Madison, WI, USA

[6]Instituto Antártico Argentino, Buenos Aires, Argentina

[7]Geophysical Institute, University of Alaska Fairbanks, Fairbanks, AK, USA,

[8]Department of Physics, University of Alaska Fairbanks, Fairbanks, AK, USA

[9]College of Earth, Ocean, and Atmospheric Sciences, Oregon State University, Corvallis, OR, USA

**correspondence to: N. Ochwat (naomi.ochwat@colorado.edu)*

Abstract

In late March 2011, landfast sea ice (hereafter, 'fast ice') formed in the northern Larsen B embayment and persisted continuously as multi-year fast ice until January 2022. In the 11 years of fast ice presence, the northern Larsen B glaciers developed extensive mélange areas and formed ice tongues that extended up to 16 km from their 2011 ice fronts. In situ measurements of ice speed on adjacent ice shelf areas spanning 2011 to 2017 show that the fast ice provided significant resistive stress to ice flow. Fast ice breakout began in January 2022, and was closely followed by retreat and break-up of both the glacier mélange and the adjacent ice tongue areas. We investigate the probable triggers for the loss of fast ice and document the initial upstream glacier responses. Our results suggest that the fast ice loss was linked to strong wave action (>1.5 m amplitude) with long period swells (>5 s) that reached the embayment simultaneously with the appearance of rifts in the ice. This coincided with a 12-year low in sea ice concentration in the northwestern Weddell Sea. Remote sensing data in the months

https://doi.org/10.5194/tc-2023-88
Preprint. Discussion started: 27 June 2023

following the fast ice break-out reveals an initial ice flow speed increase (up to 333%), elevation loss (9 to 11 m), and rapid calving of floating and grounded ice for the three main glaciers Crane (11 km), Hektoria (25 km), and Green (18 km).

1 Introduction

As the climate warms, ice shelves in Antarctica are predicted to become more susceptible to collapse (Mercer, 1978; Gilbert and Kittel, 2021). In the late 1980s and mid 1990s several ice shelves along the Antarctic Peninsula (AP) coast retreated and eventually disintegrated, including the Wordie, Prince Gustav, Larsen Inlet, Larsen A ice shelves, and in March 2002, the northern two-thirds of the Larsen B Ice Shelf (Glasser and Scambos, 2008; Cook and Vaughan, 2010). In 2008, several smaller break-up events occurred on the Wilkins Ice Shelf (Scambos et al., 2009). There has been significant research elucidating the causes of these collapses, focusing on both ice-shelf thinning due to basal and surface melting (Smith et al., 2020), as well as lake drainage mechanisms related to meltwater-induced hydrofracture (Doake and Vaughan 1991; Scambos et al., 2003; Banwell et al., 2013; Banwell and MacAyeal, 2015), plate-bending stresses on the outer-margins due to buoyancy forces (Scambos et al., 2009), and ocean swell flexure (Massom et al., 2018).

Intense surface melt events that may contribute to ice shelf collapse on the Antarctic Peninsula have been linked to atmospheric rivers (ARs; Wille et al., 2022; Wille et al., 2019) and foehn winds (Laffin et al., 2022; Datta et al., 2019; Cape et al., 2015). ARs are long narrow bands of warm and moist air that can cause extreme warm temperatures, reduce sea ice concentrations, increase ocean swell, increase surface melting (via release of latent heat and increased downwelling of longwave radiation), and set up conditions favourable for foehn events in the AP region (Wille et al., 2022; Liang et al., 2023; Bozkurt et al., 2018). Foehn events occur when a moist air mass ascends on the windward side of a mountain range and cools at the wet-adiabatic rate, while losing moisture to precipitation. It then descends over the lee side, adiabatically warming at the higher dry rate, resulting in a net increase in temperature. The dry warm air can cause large increases in melt rates (Laffin et al., 2022).

The loss of ice shelves can catastrophically reduce the stability of the outlet glaciers that once fed them, hence these outlet glaciers accelerate and thin, ultimately contributing further to sea-level rise. For example, when the Larsen B collapsed in 2002, Crane Glacier thinned by 35 m yr^{-1} (Shuman et al., 2011) and immediately sped up by roughly 3-fold (Rignot et al., 2004) and the Hektoria-Green-Evans (hereafter, HGE) Glacier system ice flow speed increased by up to 8-fold (Rignot et al., 2004), resulting in total ice losses from 2002 to 2010 of 9 Gt yr^{-1} (Berthier et al., 2012).

After the collapse of the Larsen B in 2002, the embayment supported seasonal sea ice. In late March 2011, landfast sea ice (hereafter 'fast ice') formed in the Larsen B embayment and persisted as multi-year fast ice until January 2022. Fast ice is sea ice that is attached to the shore and does not drift or move with the ocean currents or winds, it can be annual or perennial (Fraser et al., 2021). Assessments of the fast ice thickness in the Larsen B embayment near the oceanward ice front were 2.5

https://doi.org/10.5194/tc-2023-88
Preprint. Discussion started: 27 June 2023

to 4 m (Scambos et al., 2017). In the inner embayment, altimetry data indicate a thickness of tens to hundreds of meters in areas of mélange containing fast ice or glacier tongue ice (Fig. 1).

Breakout of the Larsen B multi-year fast ice began on 19 January 2022, leading, within days, to retreat and break-up of the tributary glacier mélange and floating ice tongue areas. This is because, like ice shelves, fast ice and glacier mélange are known to be stabilizers of outlet glaciers, reducing calving (Amundson et al, 2010) and/or wave action against the outlet glacier (Murty, 1985). When fast ice or mélange breaks up, ice-shelf calving resumes, sometimes releasing several decades of accumulated ice flux, and exposing the new terminus to ocean dynamics (Cassotto et al., 2015; Reeh et al., 2001). Several studies have suggested that break-up of fast ice can reduce the structural integrity of ice shelves and ultimately lead to their collapse (Banwell et al 2017; Massom et al., 2018; Borstad et al., 2013; Khazendar et al., 2007), others (Sun et al. in review) suggest that fast ice is not providing sufficient buttressing to be impactful on the system dynamics. Here we investigate the climatic and oceanic drivers that led to the increased vulnerability and subsequent break-out of the decade-old Larsen B fast ice in January 2022, while also drawing parallels to previous ice shelf collapses. We then assess the initial glacier dynamic response to the loss of the buttressing fast ice by evaluating changes in velocity, terminus position, and elevations of the Crane, Jorum, Punchbowl, and HGE glaciers.

2 Study area

The Larsen B embayment is located on the eastern side of the AP and is ~7000 km^2 in area, with a central point around 65.24° S and 61.00° W (Fig. 1). North of the embayment is the Seal Nunataks Ice Shelf (Shuman et al., 2016) and to the South is a remnant of the Larsen B Ice Shelf, now called the Scar Inlet Ice Shelf. To the west is Graham Land, a raised plateau and mountain range covered in a grounded ice cap with small outlet glaciers flowing both westward and eastward off the ridge. To the east is the northwestern Weddell Sea. Prior to 1995, the eastern coast of Graham Land was almost entirely flanked by ice shelves (e.g., Cook and Vaughan, 2010; Skvarca et al., 1999). A series of ice shelf disintegrations in the Larsen A occurred in January 1995 (e.g., Rott et al., 1996), partly attributed to warmer climate conditions flooding the surface of the ice shelves with meltwater and inducing widespread hydrofracture (Rott et al., 1998). This was followed by a larger abrupt disintegration in March 2002 of the Larsen B ice shelf due to similar causes (Banwell et al., 2013). The largest ice shelf remaining on the AP is the Larsen C Ice Shelf.

Due to the elevated narrow ridge of the northern AP (Graham Land) and the prevailing westerly wind, the climate of the region differs in its western and eastern flanks. The ridge obstructs the Southern Hemisphere westerlies and induces strong orographic lifting and precipitation on the western side, while the eastern side is much drier and cooler (King et al., 2003; Van Wessem et al., 2015). The climate is heavily influenced by the phase of the Southern Annual Mode (SAM; Fogt and Marshall, 2020; Leeson et al. 2017). When the SAM index is positive, warming events occur more frequently on the eastern side of the Peninsula due to an increase in westerly flow across the Peninsula (Van Lipzig et al., 2008; Orr et al., 2008).

https://doi.org/10.5194/tc-2023-88
Preprint. Discussion started: 27 June 2023

The Cryosphere
Discussions
Open Access

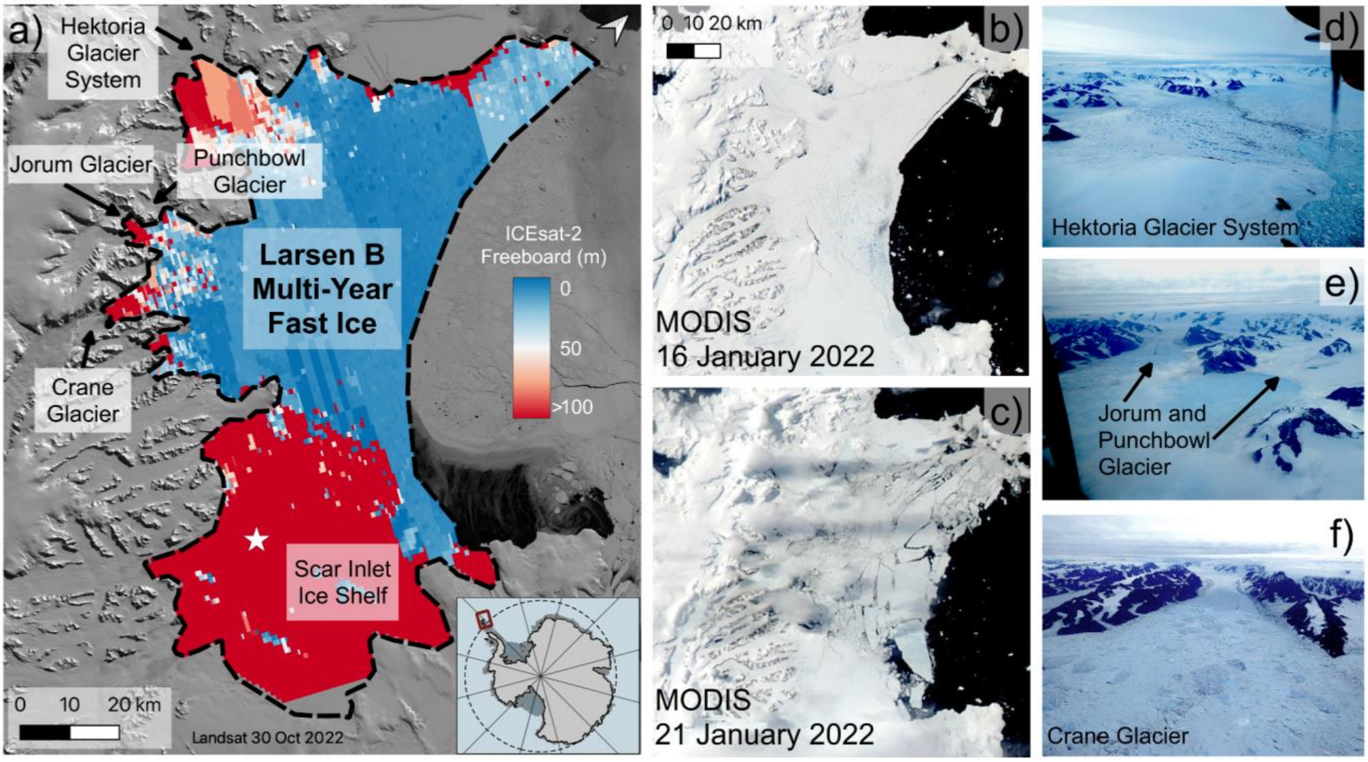

Figure 1: a) Interpolated freeboard thickness from ICESat-2 data from 2018 to late 2022. The extent of the interpolation is from the lowest fast ice extent on record in February 2019 and the inferred grounding zones (dashed black lines). AMIGOS GPS installation on Scar Inlet Ice Shelf indicated by white star, b) MODIS image from 16 January 2022 c) MODIS image from 21 January 2022, two days after initial rifts in the fast-ice formed, d, e, f) Images captured by the British Antarctic Survey on 31 January, 11 days after the fast ice break-out event.

3 Data and Methods

3.1 Reanalysis Data

We analysed climatological data to investigate why the break-out occurred during the 2021/2022 austral summer season and more specifically, on 18 to 20 January 2022. We used ERA-5 Reanalysis data, a climate reanalysis product developed by the Copernicus Climate Change Service (C3S), a part of the European Center for Medium-Range Weather Forecast (ECMWF) (Hersbach et al., 2020), at both monthly and hourly temporal resolution to assess significant trends that occurred in 2017 to 2022 and temperature and precipitation anomalies, as well as foehn wind occurrence in the months prior to January 2022. To calculate monthly anomalies, we averaged that month's climatology (1979 to 2022) then differenced the average temperature of the month in question with the climatology. To investigate the presence of foehn winds in January 2022, we followed Laffin

https://doi.org/10.5194/tc-2023-88
Preprint. Discussion started: 27 June 2023

et al. (2022), who determined that foehn winds that produce surface melt require a temperature > 0°C, a wind speed of > 2.85 m s^{-1}, humidity < 79%, and a wind direction from the N or NW.

To identify ARs during the last two weeks of January 2022, we use hourly ERA-5 to examine long filaments of vertically integrated water vapor transport (IVT) that extend from the extra-tropics towards the Antarctic ice sheet (Bozkurt et al., 2018, Wille et al., 2019). IVT is calculated as the vector magnitude of eastward integrated water vapor transport (uIVT) and northward integrated water vapor transport (vIVT). We identify an AR event during the breakout as a continuous, extended region of locally high IVT, consistent with Wille et al. (2022), that reaches a peak intensity of almost 300 kg m^{-1} s^{-1} over the Larsen B region.

To assess ocean characteristics, we used ERA-5 wave data. We used significant wave height as a proxy for wave energy (Teder et al., 2022), calculated to be four times the square root of the zeroth moment of the energy density spectrum (Massom et al., 2018). We used peak wave period for indication of longer swell periods, which can transmit more energy past the ice shelf front (Robinson and Haskell, 1992; Massom et al., 2018). We used mean wave direction for evaluating the direction of wave propagation. Here we examined an hourly time series of the variables for January 2022 in front of the Larsen B embayment and near the James Ross Island, where a wave corridor was present.

3.2 Satellite Data

3.2.1 Passive Microwave Data

To investigate changing sea ice concentrations and melt extent since 2011, we used passive microwave data from the Advanced Microwave Scanning Radiometer for the Earth Observing System (AMSR-E) on the Aqua Satellite and its successor the Advanced Microwave Scanning Radiometer 2 (AMSR-2) on the 'Shizuku' (GCOM-W1) satellite. Combined, these passive microwave sensors provide nearly continuous daily data from 2002 until present. The daily sea ice concentration data product was downloaded from the University of Bremen for 19 January on all years from 2010 to 2022 inclusive (apart from 2012, which is not available; Spreen et al., 2008) to assess sea ice concentration on the same day for the 12-year period.

We also used the AMSR-E/2 data to investigate the presence of melt on the fast ice for each melt season (October 1 to March 31) from 2011 to 2022. To do this, we followed the algorithm from Torinesi et al. (2003) and methods of Picard et al. (2007). For each 12.5 km grid cell and each day, the liquid water is detected as present if the 19 GHz horizontally-polarized brightness temperature is higher than a threshold that is empirically determined in each cell and for each year by using the brightness temperatures during the winter (dry snow) season. 'Melt days' are defined as days when meltwater is simply present on the ice surface or in the near surface, but the process of active melting is not necessarily taking place. Finally, we calculated the

https://doi.org/10.5194/tc-2023-88
Preprint. Discussion started: 27 June 2023

total number of melt days for each melt season. Compared to the fully automatic algorithm used recently in Banwell et al. (2021, 2023) for Antarctic ice shelves, here we first analyzed the time-series of brightness temperatures in all the cells close to the shore, in order to discard those contaminated by open water. This is necessary because the real footprint of the measurements acquired by the radiometer is larger than the grid cell and of elliptical shape (14 x 22 km) (Meier et al., 2018). The ellipse's position and orientation changes from track to track with respect to the grid cell. As a consequence, the fast ice grid cell near the shore may be contaminated by signal coming from the nearby open ocean; our manual selection of the grid cells assures this perturbation is small and does not affect the liquid water detection algorithm.

3.2.2 Optical Imagery and Synthetic Aperture Radar

We used several optical satellite and Synthetic Aperture Radar (SAR) imagery to assess glacier characteristics, flow speeds, melt patterns, and elevation changes. We used MODIS, Landsat 8 and 9, and Worldview (WV) -1, 2, and 3 to investigate changes in glacier morphology, meltwater lakes, and frontal positions. The MODIS sensor, on the Aqua and Terra satellites, has a data archive from 2002 to present and was used to determine the dates of break-up and retreat extents. The Landsat 8 and 9 Operational Land Imager product was used to assess melt patterns during the 2021/2022 austral season and to determine ice flow speeds using a python-based image correlation software; PyCorr (Fahnestock et al., 2016). WV-1, 2, and 3 satellite images have a very high resolution of less than 0.50 m and were used for investigating the morphology of icebergs and the creation of digital elevation models (DEMs). Worldview in-track stereo-image DEMs were obtained from the Polar Geospatial Center (PGC). The DEMs have a spatial resolution of 2 m and absolute accuracy of ~4 meters in horizontal and vertical planes (PGC documentation). These DEMs (Table S1) serve as a baseline of glacier elevation prior to, and immediately after, the fast ice break-out. We corrected for the geoid. Additionally, we assessed the mean elevation difference (i.e., bias) for six bedrock regions in each of the WV DEMs and the REMA DEM (Howat et al., 2022) and applied the mean offset to the WV DEMs, similar to the method used with the ArcticDEM for the Hunt Fjord Ice Shelf in Greenland (Ochwat et al., 2022).

We assessed calving styles and approximate grounding zone positions from all image and DEM data. The grounding zone is estimated by a break in slope in the DEMs and morphological changes such as the appearance of broad surface undulations suggestive of bottom crevassing. Calving styles of grounded ice often show surface slumping or tilting prior to separation, indicative of listric faulting (Parizek et al., 2019), super-buoyancy (Murray et al., 2015) or ice-cliff stresses (Bassis et al. 2021, Crawford et al. 2021).

We used Sentinel 1A and 1B SAR data to estimate ice flow speeds. The Alaska Satellite Facility HyP3 Pipeline uses speckle tracking to create velocity rasters using image pairs. The HyP3 pipeline utilizes GAMMA and Auto-RIFT algorithms through the Vertex On-Demand Processing Tool (Gardner et al., 2018, Lei et al., 2021). Sentinel-1A and -B imagery has a repeat time when combined of 6-days; however, Sentinel-1B malfunctioned in late December 2021, resulting in a 12-day repeat cycle starting in January 2022. For both Sentinel and Landsat derived velocities, we extracted ice speed profiles along the Airborne Thematic Mapper (ATM) from Operation IceBridge center line and along 250 m and 500 m lateral offsets, for Crane, Jorum, Green, and Hektoria glaciers, generating five profiles that span the central 1 km across the approximate glacier centerlines. We averaged these profiles for the five lines. To approximate the mean monthly speed, we averaged the speed profile of two 12-day cycles.

3.2.3 Laser Altimetry

To study changes in surface ice elevation, we combined the DEMs from WV imagery with ICESat-2 altimetry data. We used the ICESat-2 ATL06 version 5 product, which provides a linear surface approximation of 40 m overlapping segments along each ground track (Smith and others, 2021) with a 91-day repeat cycle (clouds permitting). We correct for the geoid prior to estimating the initial thickness of the fast ice, glacier tongues, and elevation of the glaciers. We interpolated ICESat-2 data for the period September 2021 to December 2022 (Fig. 1) for initial fast ice and glacier tongue freeboard. Assuming snow is negligible, we calculated fast ice thicknesses from the freeboard using the standard hydrostatic equilibrium floating ice relationship using a density of 1028 kg m^{-3} for sea water and 900 kg m^{-3} for ice. For analysing the elevation changes, we extracted ICESat-2 data from where tracks cross <200 m of near-centerline tracks flown by Operation IceBridge using the ATM sensor, then we averaged the data. Standard error analysis was performed on the individual WV and ICESat-2 elevations; we use the square-root of the sum of the squares of the error, where the errors are the standard error of the mean and the instrument error of WV or ICESat-2.

3.2.4 GNSS data from AMIGOS station on Scar Inlet

An Automated Meteorology-Ice-Geophysics Observing System (AMIGOS) unit with a dual-channel GPS receiver was placed on the Scar Inlet Ice Shelf in February of 2010 (Larsen Ice Shelf System, Antarctica; LARISSA; Wellner et al., 2019; Scambos et al., 2013). The system provided hourly position data spanning February 2010 through August 2017, with several data gaps due to power and system malfunctions, which were periodically repaired during re-visits. Precision of the hourly position data was approximately ±20 cm due to wind on the tower mounting of the GPS antenna. We used daily, weekly, and monthly averaged data to evaluate ice flow of the Scar Inlet Ice Shelf over the formation and thickening period of the adjacent fast ice.

3.2.5 Aerial photography

To evaluate how the fast ice break-up occurred and the potential calving styles of the outlet glaciers, we also analysed airborne photography. On 31 January 2022, the British Antarctic Survey flew a Twin Otter over the study area with a digital camera (Panasonic DMC-TZ80e) and a series of photos were taken along with approximate geolocation.

https://doi.org/10.5194/tc-2023-88
Preprint. Discussion started: 27 June 2023

The Cryosphere Discussions

4 Results

4.1 Multi-year fast ice in the Larsen B embayment

4.1.1 Formation and evolution of Larsen B multi-year fast ice

In March 2011, pack ice in the Larsen B embayment froze in place, forming the fast ice cover that persisted until mid-January 2022. Portions of the fast ice broke out and reformed in May 2011 and March 2012. From March 2012 onwards, the fast ice maintained a minimum area of ~3975 km^2 according to the MODIS record. From 2012 to 2016 the fast ice was relatively stable with a maximum area of ~6280 km^2 in 2016. After 2016, the eastern edge of the fast ice, which was ~1200 km^2 in area, seasonally re-formed and broke-out, while the inner portion of the fast ice remained intact. The lowest extent on the MODIS record was in February 2019, when a slightly larger portion (2000 km^2) of the outer edge broke out. From 2020 to early 2021, the sea ice partially recovered in area from the 2019 low point and was within 600 km^2 of the 2016 sea ice area. However, in late 2021 the edge broke out again, returning to the 2019 areal extent. In 2022, prior to the fast ice break-out event, the extent was most similar to the 2019 minimum.

4.1.2 Upstream glacier response to fast ice formation

During the period of fast ice occupation in the embayment, our analysis suggests that the fast ice temporarily stabilized the Larsen B tributary glacier fronts and buttressed the Scar Inlet Ice Shelf. Based on the MODIS and Landsat satellite image record, the glacier tongues readvanced into the embayment, their fronts becoming a floating composite of glacier ice, large icebergs, and sea ice. This assortment of ice reached thicknesses up to 320 m near glacier termini (inferred from freeboard estimates in Fig. 1 and assuming hydrostatic equilibrium). Crane's terminus and associated mélange advanced at ~1 km yr^{-1} (11 km total) and the trunk of the glacier thickened, likely from increased ice input from the thinning tributary glaciers (Needell and Holschuh, 2023). The HGE system and mélange reformed an ice-shelf-like feature with a freeboard exceeding 40 m (Fig. 1). Additionally, this system advanced approximately 16 km since February 2011. Jorum Glacier advanced ~4.5 km over the same period, however Punchbowl Glacier only readvanced ~0.5 km and did not create an extensive mélange or glacier tongue compared to the HGE system or Crane Glacier.

GPS data from Scar Inlet Ice Shelf (Fig. 2) show an acceleration of ice shelf flow speed from installation of the GPS in early 2010 to late 2012, followed by a generally stable flow speed with a seasonal cycle. This indicates that the ice shelf was accelerating prior to the formation and thickening of the multi-year fast ice. From late 2012 onwards, the acceleration of the ice shelf was halted, two years after the fast ice began its occupation, indicating a significant buttressing of the ice shelf and presumably the glacier fronts, since the ice shelf would be expected to increase in speed along an unobstructed flowline.

https://doi.org/10.5194/tc-2023-88
Preprint. Discussion started: 27 June 2023

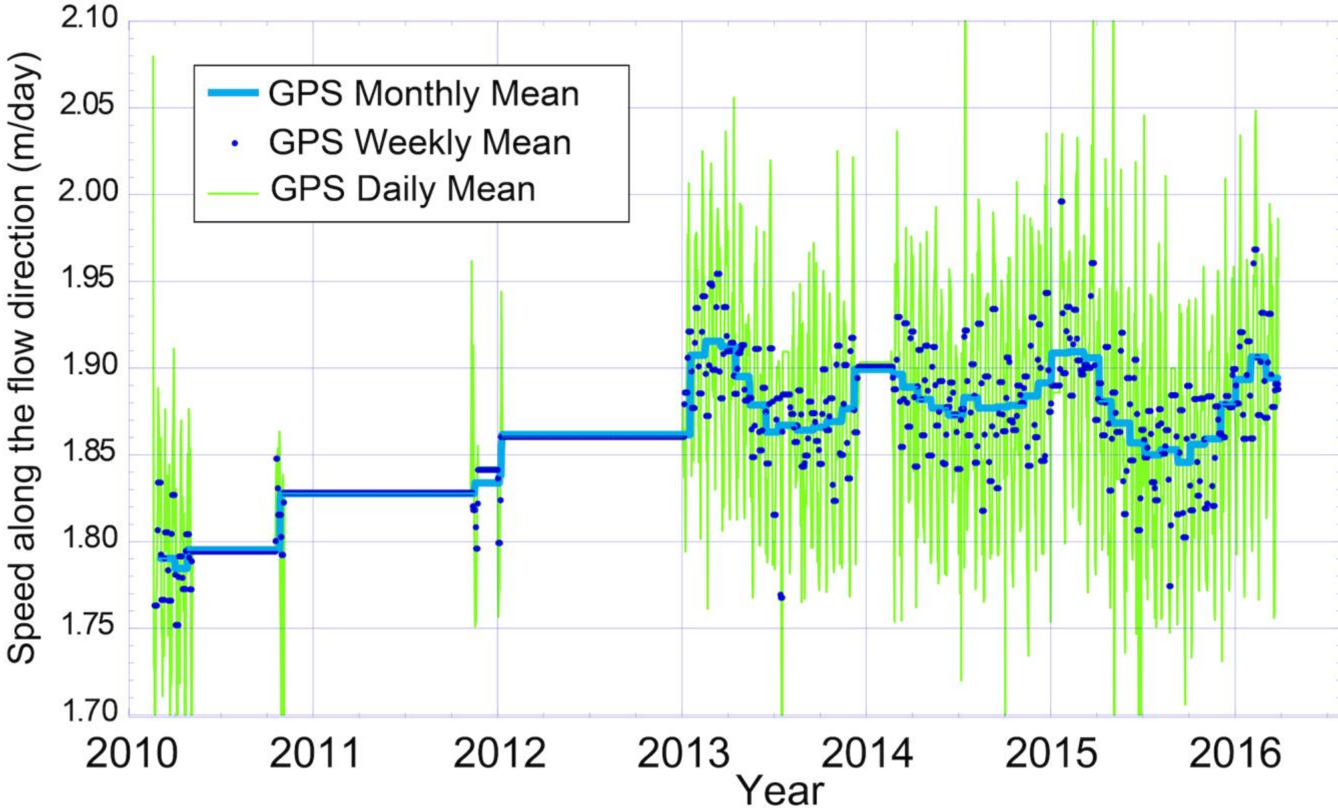

Figure 2: Scar Inlet Ice Shelf ice flow speeds from AMIGOS GPS from 2010 to 2017. Blue line is the monthly mean, blue points are the weekly means, and green vertical lines are the daily means.

4.1.3 Multi-year fast ice break-up

MODIS imagery and Fig. 1b and c, shows that narrow fractures started to form in the fast ice between 18 and 19 January 2022, widening thereafter, and by 20 January the whole area of the fast ice was fully fractured. By 21 January, the fast ice had drifted 9 to 16 km northeast out of the embayment and into the Weddell Sea, exposing the tributary glacier fronts to the open water in the Larsen B embayment (Fig. 1c). The fast ice floes continued to drift away, fully clearing and leaving open water in the embayment by 8 February.

Sea ice began to re-enter the embayment in late February 2022, but sea ice cover was not persistent through the next 13 months. Over the course of the late austral summer into the autumn and winter, MODIS images indicate sea ice cover in the embayment varied in extent and apparent coherency. Open water conditions in the embayment and the area adjacent to the AP and James Ross Island persisted through March 2022. Landfast ice did not form in the embayment during the 2022 autumn and winter. The sea ice concentration varied in October 2022, began to decrease in November 2022, and by December 2022 there were

https://doi.org/10.5194/tc-2023-88
Preprint. Discussion started: 27 June 2023

minimal floating bergs or sea ice plates. From January to March 2023 the embayment was devoid of floating ice and remained open ocean. However, by the end of March 2023, sea ice started to reform in the embayment.

4.2 Potential Attributions of the 2021-2022 Fast Ice Breakout

4.2.1 Seasonal climate conditions

To understand climate conditions that may have affected the vulnerability of the fast ice, we explored wind speed, precipitation, and temperature anomalies (compared to the 1979 to 2022 climatology) for the months leading up to the start of the fast ice break-up event in January 2022, as well as the presence of ARs and foehn winds. For November 2021 to January 2022, there is no substantial total precipitation anomaly in our study area (Fig. S1A). The wind speed anomaly composites suggest a slightly higher than average wind speed throughout most of the 2021/2022 melt season, with December having the largest anomaly, primarily in the Bellingshausen Sea area near the Western AP (Fig. S1B). The temperature anomaly over this time period indicates the Bellingshausen Sea was slightly warmer (~2°C) than the 1979 to 2022 climatological average, whereas the Larsen B embayment was up to 4°C warmer (Fig. 3).

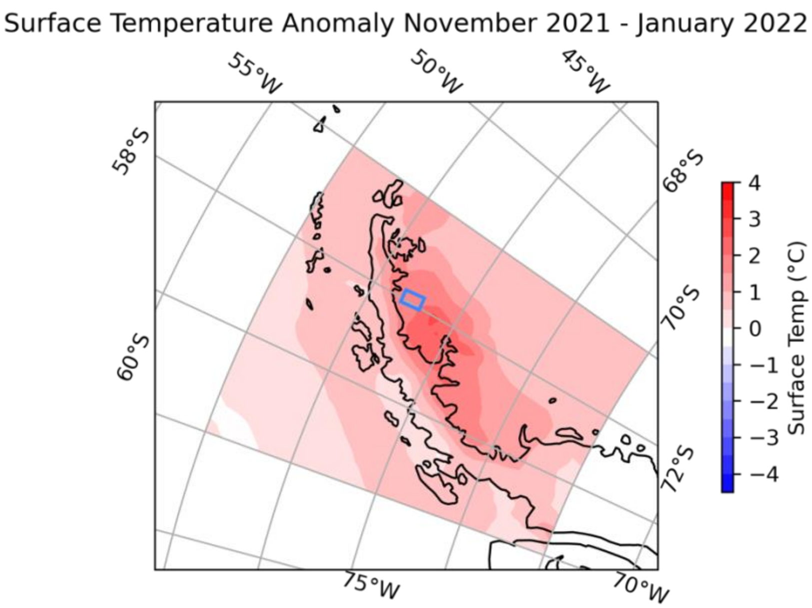

Figure 3: ERA-5 surface temperature anomalies around the Antarctic Peninsula. The blue box is the area of grid cells used for the foehn wind analysis (Fig. S2).

We also looked at a time series of several meteorological variables that indicate foehn wind events, such as temperature, relative humidity, snow evaporation, windspeed, and wind direction (Fig. S2). The time series shows the mean hourly data of the four grid cells (blue box, Fig. 3) from the Larsen B embayment for January 2022. A series of five foehn wind events

https://doi.org/10.5194/tc-2023-88
Preprint. Discussion started: 27 June 2023

occurred from 17 to 21 January 2022, two prior to the event, one during, and two after. This suggests a foehn wind event was occurring, enhancing surface melt on the fast ice, potentially causing a perpetuation of the break-up and in the later events (19 and 21 January) aiding in the dispersal of the fast ice from the Larsen B embayment into the Weddell Sea.

Since ARs may be linked to foehn events and increased surface melt from latent heat and enhanced downwelling longwave radiation (Bozkurt et al., 2018), we also investigated whether or not there was an AR in the period of the fast ice break-out event. We find a long, narrow band of high IVT that extends from the eastern Pacific across the Drake Passage and into the Atlantic Ocean, indicating the presence of an AR (Fig. 4a; Wille et al., 2022). A time series of IVT in the Larsen B region (65.25°S, 61.25°W) indicates that IVT associated with the AR event begins to increase on 19 January and peaks on 20 January 11:00 UTC (Fig. 4b). IVT remains high until 22 January, when the AR weakens and dissipates.This event occurred simultaneously as the distinct foehn events from 19 to 22 January, suggesting the AR occurred after the initiation of the break-out, was a driver for the foehn event, and potentially assisted in the dispersal of the fast ice.

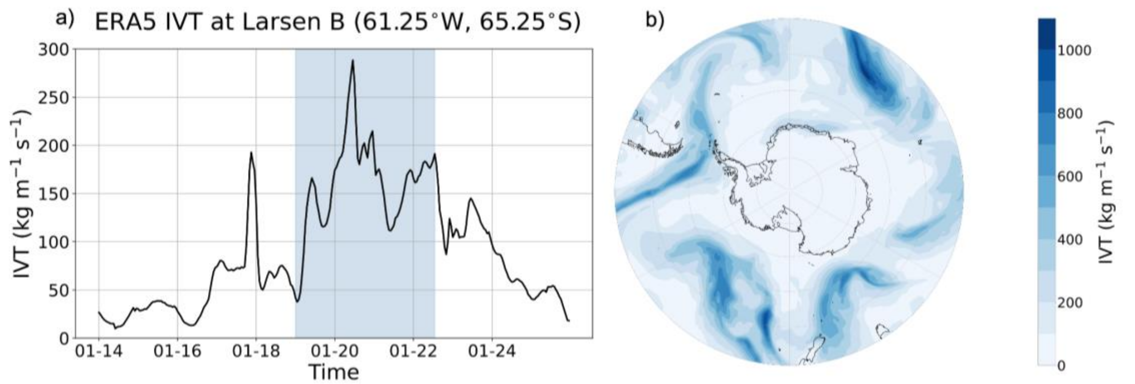

Figure 4: a) time series of IVT for January 2022 at 65.25°S, 61.25°W. b) map of ERA-5 vertically integrated water vapor transport (IVT)in the southern hemisphere at 11:00 UTC on 20 January 2022, during the peak IVT at Larsen B. The AR is identified as a long filament of high IVT that extends from the eastern Pacific across the Antarctic Peninsula and into the Atlantic Ocean.Blue shading indicates the duration of the AR event over Larsen B.

4.2.2 Surface melt

Fig. 5 shows cumulative melt days for each melt season from 2012/2013 to 2020/2021 over the Larsen B multi-year fast ice and Scar Inlet Ice Shelf, derived from AMSR-E/2 passive microwave data. Fig. 5a shows a map of the grid cells used in the analysis, as well as cumulative melt days for the 2019/2020 season, 2020/2021 season (i.e. the two melt seasons preceding the break-up event), and the mean cumulative melt days for each season from 2012/2013 to 2020/2021. We do not include the 2021/2022 melt day data in Fig. 5a because the mid-season break out of the fast ice resulted in mixed surface and open water grid cells, preventing the melt detection. Maps of cumulative melt days for all melt seasons are available in Fig. S3. Fig. 5b

https://doi.org/10.5194/tc-2023-88
Preprint. Discussion started: 27 June 2023

shows the spatially-averaged melt days over the study area, as well as the cumulative days when the melt area was 100% of the study area, for nine melt seasons leading up to the break-up event, as well as the melt season with the fast ice break-out (2021/2022). For both these aforementioned metrics, the 2021/2022 season did not have a long nor spatially extensive melt season relative to the previous nine melt seasons. 2019/2020 was both the longest melt season and the one with the highest number of days with 100% melt area, nonetheless the fast ice survived this season, as well as the preceding high-melt years.

In addition to our analysis of passive microwave data (above), which may indicate the presence of surface meltwater ponding (e.g. Picard et al., 2022), we also analyzed optical satellite images for evidence of surface meltwater ponding, including Landsat 8. Landsat 8 images in November and December 2021 show the surface of the fast ice was extensively covered with melt ponds (Fig. S4). However, by January 2022, the surface melt ponds on the fast ice appeared to have refrozen, with reduced melt pond coverage (Fig. S4).

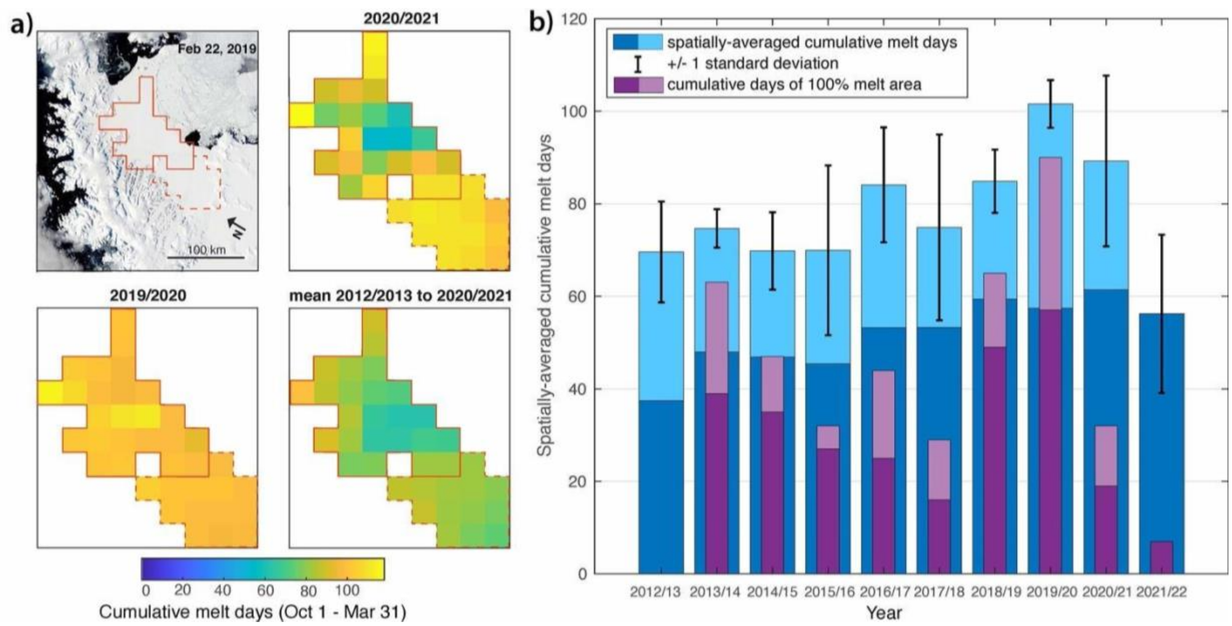

Figure 5: Cumulative melt days derived from AMSR-E/2 passive microwave melt data. a) Cumulative melt days over the fast ice area in the Larsen B embayment (area within solid red lines) and over the Scar Inlet Ice Shelf (area within dashed red line) for the 2019/2020 and 2020/2021 melt seasons, and the mean from 2012/2013 to 2020/2021. b) Spatially-averaged melt days (blue shades) and cumulative days of 100% melt area (purple shades) over just the Larsen B embayment fast ice (solid red lines in panel a) from 2012/2013 to 2021/2022. The dark purple and dark blue bars show cumulative melt days from just 1 October through 18 January (i.e. the only data available for the 2021/2022 season), and the light purple and light blue bars show cumulative melt days from 1 October through 31 March.

https://doi.org/10.5194/tc-2023-88
Preprint. Discussion started: 27 June 2023

4.2.3 Sea ice

Fig. 6a displays a map of sea ice concentration from AMSR-E/2 data in the vicinity of the Larsen B embayment on 19 January 2022. Fig. 6b shows a time series of sea ice extent (concentration multiplied by area of pixel) for the date of 19 January for each year from 2010 to 2022 (except 2011/2012, when AMSR-E/2 sensor data are not available) in a selected region (gray box in Fig. 6a). The selected region represents a potential ocean swell corridor leading to the Larsen B embayment from 2010 to 2022 (see Section 5.2). For the 8-year period (2013 to 2020 inclusive) the sea ice extent in this region of the northwest Weddell Sea was over 125,000 km^2 (>50% of the box area). In 2011, sea ice extent was just 100,000 km^2 on 19 January; however, we note that the fast ice formed later in this year (March). The sea ice dropped in 2021 to 75,000 km^2, and in 2022 its area was just below 40,000 km^2. As Fig. 6a shows, a corridor is present along the eastern side of the Peninsula in January 2022, which opened on ~8 January 2022 according to the MODIS and AMSR-E/2 record. This pathway, which allows for wave action to access the front of the Larsen B fast ice, had not been present since the fast ice's formation in 2011 (Figs. 6b and S5).

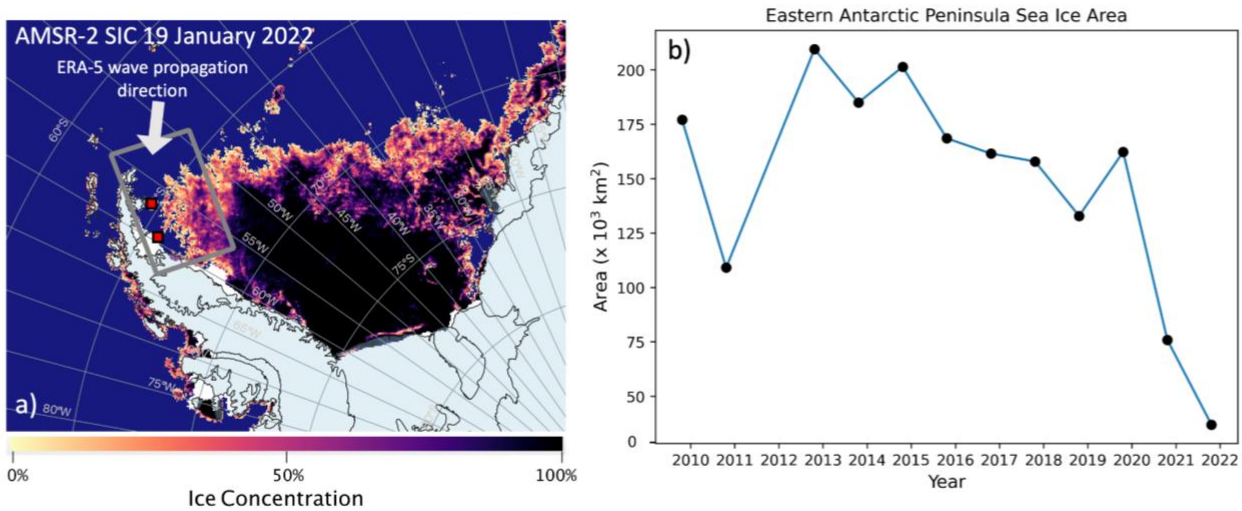

Figure 6: a) Sea ice concentration and distribution map on 19 January 2022 from AMSR-2 data (Spreen et al., 2008). Small red squares show the location of the ERA-5 wave height grid cells (Fig. 7). The gray box is the region selected for the sea ice area in 6b. The white arrow denotes the wave propagation direction on 19 January ERA-5 data; b) sea ice area from AMSR-E and AMSR-2 data in the corridor region of the NW Weddell Sea for 2010 to 2022, error in sea ice concentration according to Spreen et al., (2008) is ~7%.

4.2.4 Wave action

Examining both ERA-5 and WaveWatch-III wave data, the first large swell able to pass through the wave corridor and reach the Larsen B fast ice edge occurred on 18 and 19 January (Figs. 7 and S6). In the early hours (UTC) of 18 January 2022, the significant wave height averaged ~0.1 m in the selected grid cell region. By the afternoon on 18 January the average wave

https://doi.org/10.5194/tc-2023-88
Preprint. Discussion started: 27 June 2023

height then rose steeply to a maximum of 1.75 m near Larsen B and to over 2 m near James Ross Island ~150 km to the northeast (red boxes, Fig. 6). Simultaneously, the peak wave period rose to ~5 s, which suggests a wavelength of ~40 m. The wave propagation direction was bearing ~250° ± 25° through this period, similar to the orientation of the open corridor in the sea ice. There were not any events in November or December 2021 that included both a long peak period and a high significant wave height. Both months have peak periods consistently less than 6 s and wave heights below 1.4 m (Fig. S7). Furthermore, there were no other times during January 2022 when the wave swell had both a long peak period and high significant wave height (Fig. 7). Abrupt shifts in peak period and significant wave height (see Methods) are evident when the wave corridor opens near James Ross Island (gray band 8 Jan 2022) and when the event occurs (gray band 18 Jan 2022), as well as when the wind direction changes (Fig. S2).

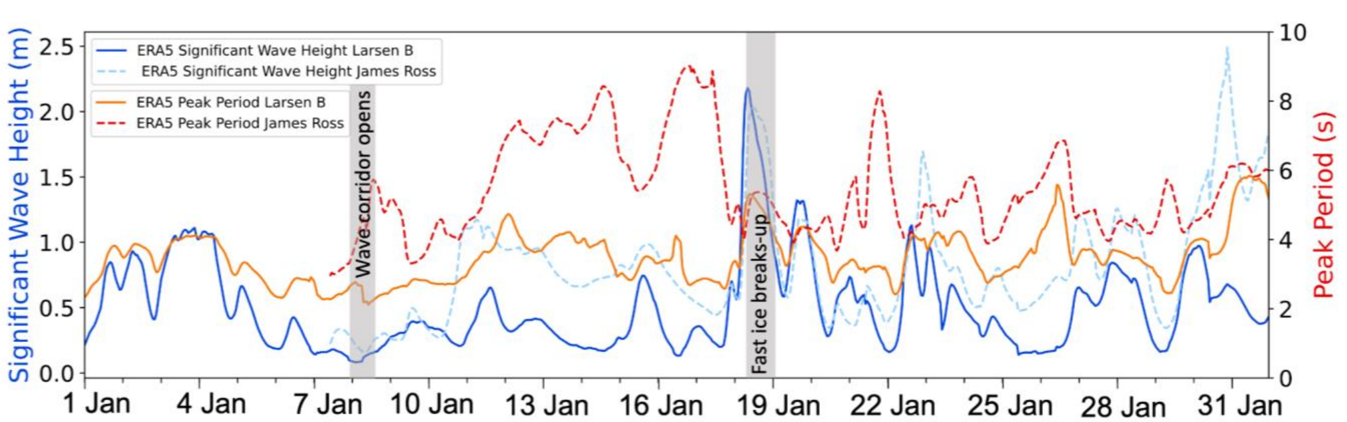

Figure 7: ERA-5 significant wave height and peak period for both the Larsen B area and near James Ross Island (dashed lines) during January 2022. The red and dark red lines and the blue and light blue lines correspond to the peak period and significant wave height, respectively. The opening of the wave corridor and fast ice break-up are denoted by the gray bands.

4.3 Initial glacier response to fast ice break-out

4.3.1 Initial retreats of landfast ice and glacier fronts

Four main upstream glaciers experienced varying immediate responses to the fast ice break-out. Crane and Jorum Glaciers exhibited similar responses, losing most of their floating ice tongues within days of the fast ice breakout (Fig. 8a). They calved large (several km^2) full-thickness tabular icebergs. Once the floating portion was removed, both glaciers underwent buoyancy-driven calving and tidewater-style retreat at their grounding zones, evident by the presence of toppled icebergs in optical images and high-backscatter iceberg surfaces in Sentinel-1 data. Scattering intensity is related to surface roughness as well as how much melt has affected the surface of the berg; freshly toppled cold bergs will have a brighter surface, whereas tabular bergs that have been exposed to surface melt will display a decreased backscatter intensity (Young et al., 1998). Punchbowl Glacier began calving in a style that appears to be buoyant full thickness calving (Murray et al., 2015), indicated by toppled

https://doi.org/10.5194/tc-2023-88
Preprint. Discussion started: 27 June 2023

dark blue icebergs. Unlike Crane, Jorum, and HGE, Punchbowl did not readvance into the embayment during the fast-ice occupation. Hektoria and Green Glacier retained a 13 km extended thick (greater than 300 m) floating tongue after the immediate break-out, until March 2022. Once Hektoria and Green Glaciers began losing their merged floating tongue in March 2022, the floating ice also underwent full-thickness tabular calving with occasional toppled icebergs (Fig. 8). From April to October 2022 the ice fronts were relatively stable, but rapid retreat reinitiated in November 2022. The calving style resembled tidewater glacier retreat for grounded ice, similar to the Röhss Glacier response from the loss of the Prince Gustav Ice Shelf (Glasser et al., 2011) or calving regimes at Helheim Glacier, Greenland (Murray et al., 2015).

In the weeks and months following the start of the fast ice break-up, Crane, Jorum, and Punchbowl glaciers continued to retreat. By 8 February 2022 the Crane Glacier floating front (defined as the limit of contiguous ice greater than 100 m in thickness; consistent with Needell and Holschuh, 2022) had retreated more than 6.5 km and was still calving large tabular bergs (several km^2 and greater than 300 m thick, based on DEMs; Fig. 8a). From 8 February until 11 March 2022 only 400 to 800 m of retreat occurred. From 16 March until 27 August 2022 Crane retreated another 1.2 km, and from 27 August to 3 September, another 400 m was calved (Fig. 8a). Then Crane restabilized and did not lose any more of its front until November 2022 when it lost only a few hundred more meters. In December 2022 another 600 m were lost during two separate events. Crane briefly stabilized from January to March 2023, yet another 800 m retreat occurred from 13 March to 7 April 2023 (Fig. 8a). Its retreat totalled ~11 km, of which possibly 1 to 2 km was grounded ice (Fig. 8b). Similar to Crane in calving style, the Jorum Glacier main trunk lost ~5 km of floating ice and its (former) tributary branch glacier lost ~6 km. Punchbowl Glacier, in contrast, has only lost a few hundred meters of its ice front as of May 1 2023.

Hektoria and Green Glacier responded to the collapse in later months following the fast ice break-out. Hektoria Glacier had an extended thick (>300 m) floating tongue (Fig. 8c) that persisted until 12 to 17 March 2022, when it retreated ~7 km (Fig. 8c). From 26 to 30 March, Hektoria's tongue retreated another ~6 km, exposing an arcuate ice front. From April 2022 until August Hektoria's ice front retreated ~1 km, inferred to be from grounded ice based on calving style and surface morphology changes. For all of September and October Hektoria's front did not change. Hektoria retreated ~3 km by 14 November and another 1.2 km by 30 November 2022. In December 2022 Hektoria underwent another series of retreats totaling ~4 km. From 17 January to 15 March 2023, another ~1.5 km retreat into the fjord occurred, and Hektoria is still actively retreating as of April 2023 and has retreated a total of ~25 km, of which ~10 km may have been grounded ice (Fig. 8d). Green Glacier has

https://doi.org/10.5194/tc-2023-88
Preprint. Discussion started: 27 June 2023

The Cryosphere Discussions

also retreated substantially but not as far into its fjord. Following a similar timeline to Hektoria, Green has retreated ~18 km total.

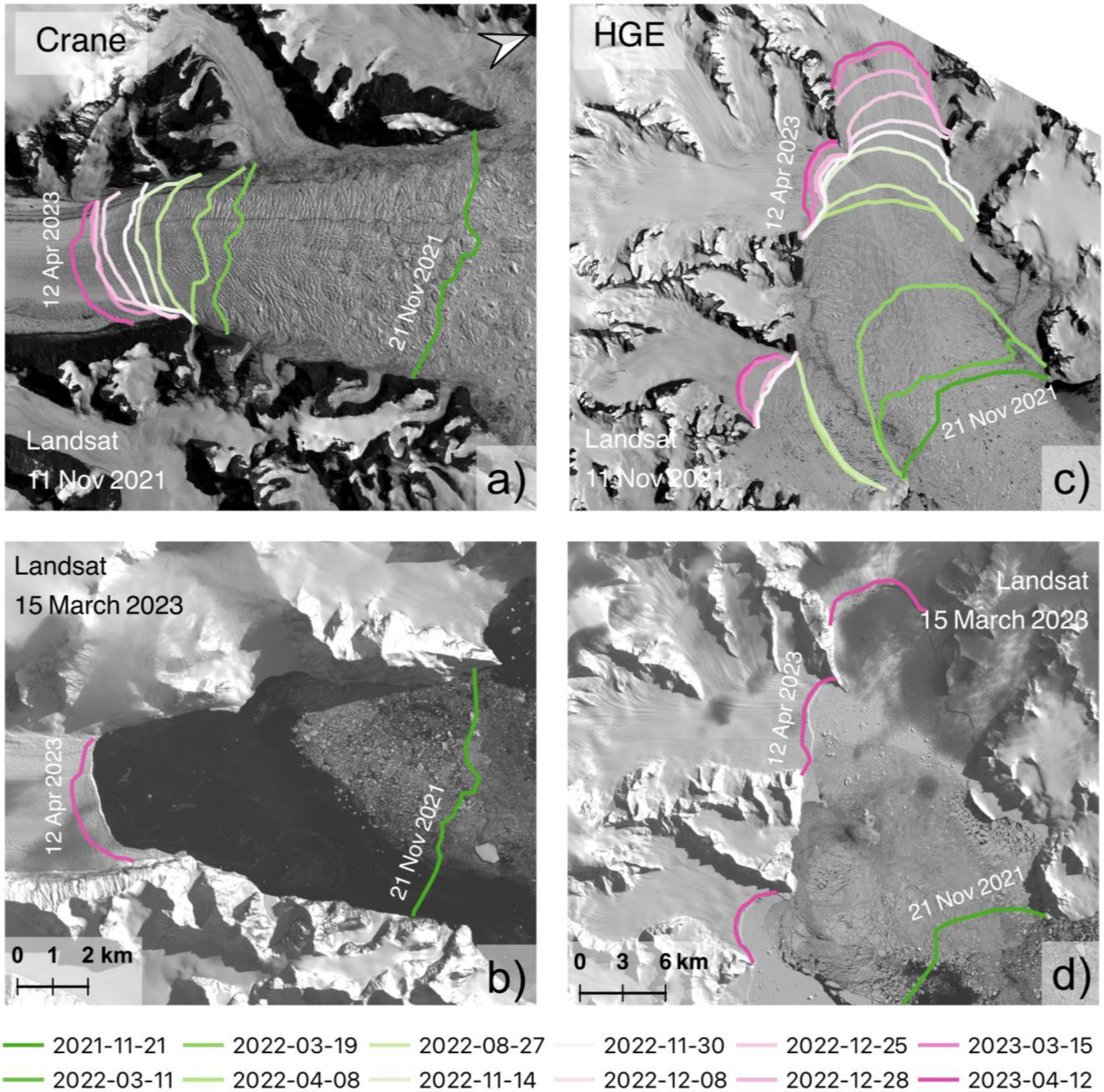

https://doi.org/10.5194/tc-2023-88
Preprint. Discussion started: 27 June 2023

The Cryosphere Discussions

Figure 8: a) Crane Glacier retreat fronts from November 2021 to April 2023 b) Crane Glacier with pre-break out terminus position and April 2023 terminus position c) HGE system retreat fronts from November 2021 to April 2023 d) HGE system with pre-break out terminus position and April 2023 terminus position. For a) and c) the background is Landsat from 21 November 2021 and for b) and d) the background is Landsat from 15 March 2023

4.3.2 Glacier centerline speed changes

Initial ice flow speed profiles along near-centerline tracks of Crane, Jorum, Green and Hektoria glaciers all show an increase in speed of various magnitudes since the fast-ice break-out event. For all the glaciers besides Punchbowl, the floating portions increased in speed dramatically immediately after the break-out event while the grounded portion of the glaciers took many months to be affected. We inferred the location of the grounding zone on the basis of crevasses, surface depressions, and rift patterns, and the surface slope using REMA and WV-2 and -3 DEMs (Fig. 9a-c; gray shaded bands on profiles and dashed white lines on insets). Additionally, the observed speed changes over a 26-month period (January 2021 to March 2023) have a distinct break in dynamics at the grounding zone, with far less change above noise levels in the data upstream of that boundary.

The Crane Glacier tongue accelerated and extended along-flow immediately after the event leading to an increase of speed from 1000 m yr^{-1} to 1300 m yr^{-1} within the first two months (Fig. 9a; light blue to yellow-green solid lines). The grounded portion of Crane Glacier responded in the months following. By November 2022 the grounded ice speed increased from 800 to 900 m yr^{-1} (Fig. 9a; yellow to dark-yellow solid lines) and by March 2023 the speed was 1200 m yr^{-1} (Fig. 9a; red solid lines). Crane Glacier is still undergoing retreat and acceleration as of March 2023.

Jorum Glacier did not experience as dramatic a change in speed after the event. Jorum Glacier has three distinct speed regimes: the upper glacier is slow-moving at 100 to 200 m yr^{-1}, the glacier's steep portion is 500 m yr^{-1} over a distance of 1.5 km, the lower glacier hovered around 500 m yr^{-1} prior to the break-out (Fig. S8). By November 2022, this lower section had increased in speed by ~75 to 100 m yr^{-1}, and has remained at ~500 m yr^{-1} as of March 2023 (Fig. S8). Jorum Glacier's floating tongue quickly calved away after the event so the floating icebergs and loose mélange were not tracked for speed.

The HGE system experienced significant changes after the break-up of the fast ice. The floating portion of the system did not experience speed changes after the loss of the fast ice (Fig. 9a-c; January to March 2022; light blue to yellow-green solid lines). However, the floating tongue was removed by April 2022 leaving only grounded ice. The mélange speed is occasionally tracked when it is cohesive (solid lines downstream of grounded line from April 2022 onwards). Speed changes occurred in both the main trunk of Green and Hektoria Glacier. Green Glacier increased in speed by January 2023 going from ~500 m yr^{-1} up to 1150 m yr^{-1}. Green Glacier's SAR-derived and Landsat-derived ice speeds for December 2022 and January 2023 agree in the general trend (Fig. 9b; light brown and brown solid lines). Hektoria Glacier's Landsat-derived ice speeds show a velocity

https://doi.org/10.5194/tc-2023-88
Preprint. Discussion started: 27 June 2023

increase from September 2022 to March 2023 from 300 m yr^{-1} to 1200 to 1400 m yr^{-1} (Fig. 9c; light brown and brown solid lines). Both Green and Hektoria are still undergoing retreat and acceleration as of March 2023.

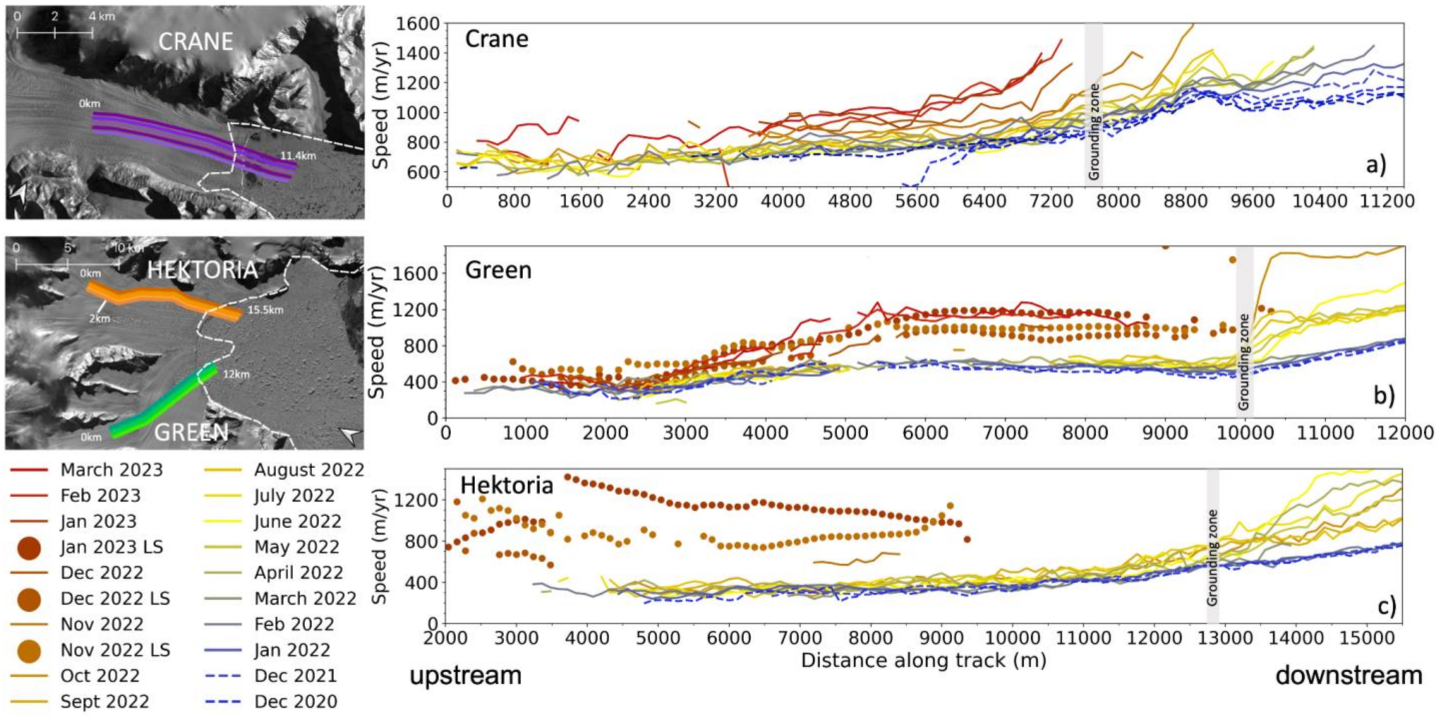

Figure 9: ATM centerline monthly averaged speeds derived from Sentinel-1 speckle tracking from Alaska Satellite Facility HYP3-pipeline, solid-colored lines. PyCorr derived speeds from Landsat imagery are the colored solid dots. Gray bands on profiles and dashed white line on image insets show inferred grounding zones. a) Crane Glacier velocity profile b) Green Glacier velocity profile c) Hektoria Glacier velocity profile, note the distance along track begins at 2000 m due to absent velocity data. Blue dashed lines are reference years Dec 2021 and Dec 2020, prior to break-out. Floating portions accelerate after break-out (March to May 2022, yellow and yellow-green solid lines). Grounded ice for all the glaciers accelerates obviously by November 2022 (light brown solid lines). February and March 2023 (red and red brown solid lines) have the largest acceleration for all glaciers. Image background is Landsat 06 October 2022.

4.3.3 Elevation changes

We used ICESat-2 altimetry and WV-1, -2, and -3 stereo-image DEMs to assess elevation changes of the Larsen B embayment glaciers from 2017 to present. For each glacier, we analyzed three reference points along the near-centerline to these changes. Lower Crane Glacier (red box, Fig. 10) may have thinned by up to 16 m immediately after the fast ice break-out, however the trend is incomplete due to the glacier's retreat and the analysis point calving off. The middle and upper section of Crane (orange and blue box, Fig. 10) shows a thickening from 2017 to 2022, consistent with Needell and Holschuh's (2023) findings. Thinning may have been initiated in those regions, however the data are inconclusive, as the thinning is only 1 to 3 m as of

https://doi.org/10.5194/tc-2023-88
Preprint. Discussion started: 27 June 2023

February 2023, which is within the natural variability of the glacier surface and measurement error. Jorum and Punchbowl glaciers show inconclusive results as well, with high amounts of variability within the available data (Fig. S9).

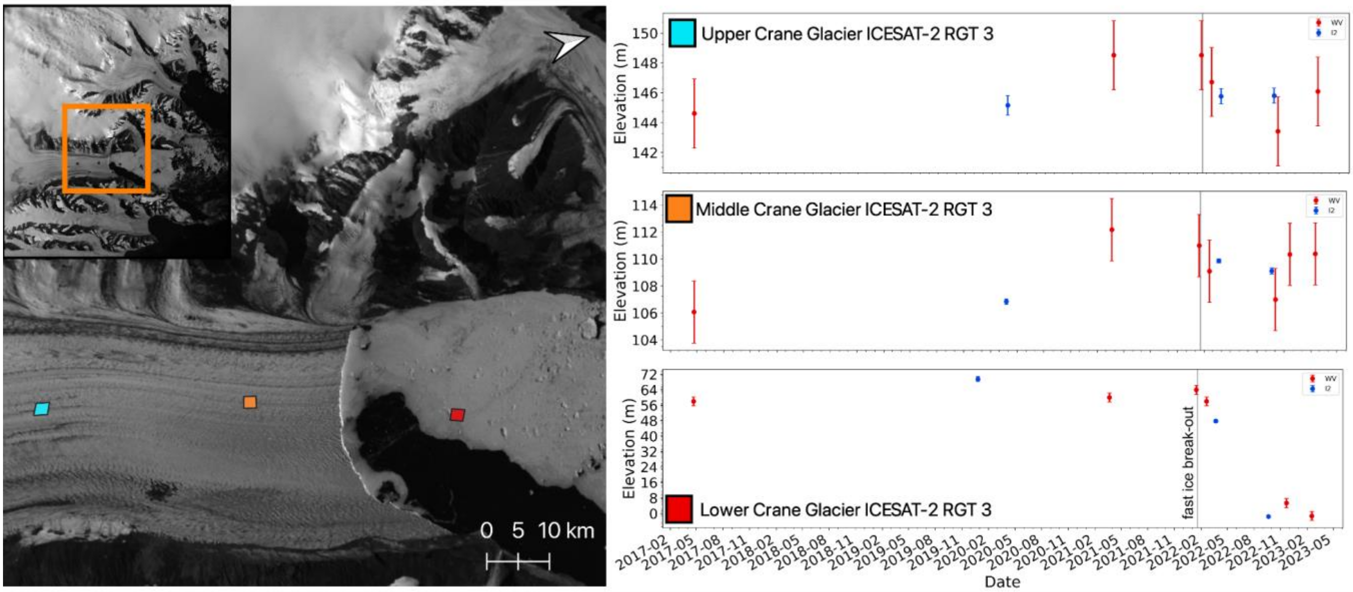

Figure 10: Crane Glacier near-centerline elevation changes through time. Background image is from 17 January 2023 Landsat. The time series plot corresponds to the area of the box of the same color. The gray band indicates the date of the fast ice break-out event. Note the different vertical scales on the figure.

The HGE system shows thinning in various regions and dramatic elevation change when parts of the system calve away. Fig. 11 (yellow box) shows the HGE system floating tongue freeboard as 40 m, which is ~320 m thick ice assuming hydrostatic equilibrium. After the break-out event icebergs are present in the data (>5 m freeboard) until the open ocean period (December 2022). Hektoria Glacier lacks long-term elevation change data points, simply because the regions that were picked to evaluate elevation calved and collapsed before a repeat elevation measurement of the glacier surface could be made (blue and green boxes; Fig. 11). The upper portion of Hektoria (dark orange box; Fig. 11) appears to have thinned since early 2018 (or prior). Minimal thinning occurred from April 2022 to late December 2022. As of 06 April 2023, this portion of the glacier is currently 400 m from the rapidly-retreating glacier terminus and is unlikely to remain a useful elevation measurement site. Both the lower and upper Green Glacier (orange and blue boxes, respectively; Fig. 11) show obvious thinning outside of the variability from 2017-present. Lower Green Glacier thinned ~11 m between March 2022 to late December 2022, going from 79 m to 68 ±2.3 m. Upper Green Glacier thinned ~9 m between January 2021 to late December 2022, going from 162 ±0.5 m to 153 ±2.3

m. There are no data available between January 2021 and July 2022, so the initiation of thinning of the glacier is uncertain. However, from July 2022 until late December 2022, ~5 m of the total 9 m of thinning occurred.

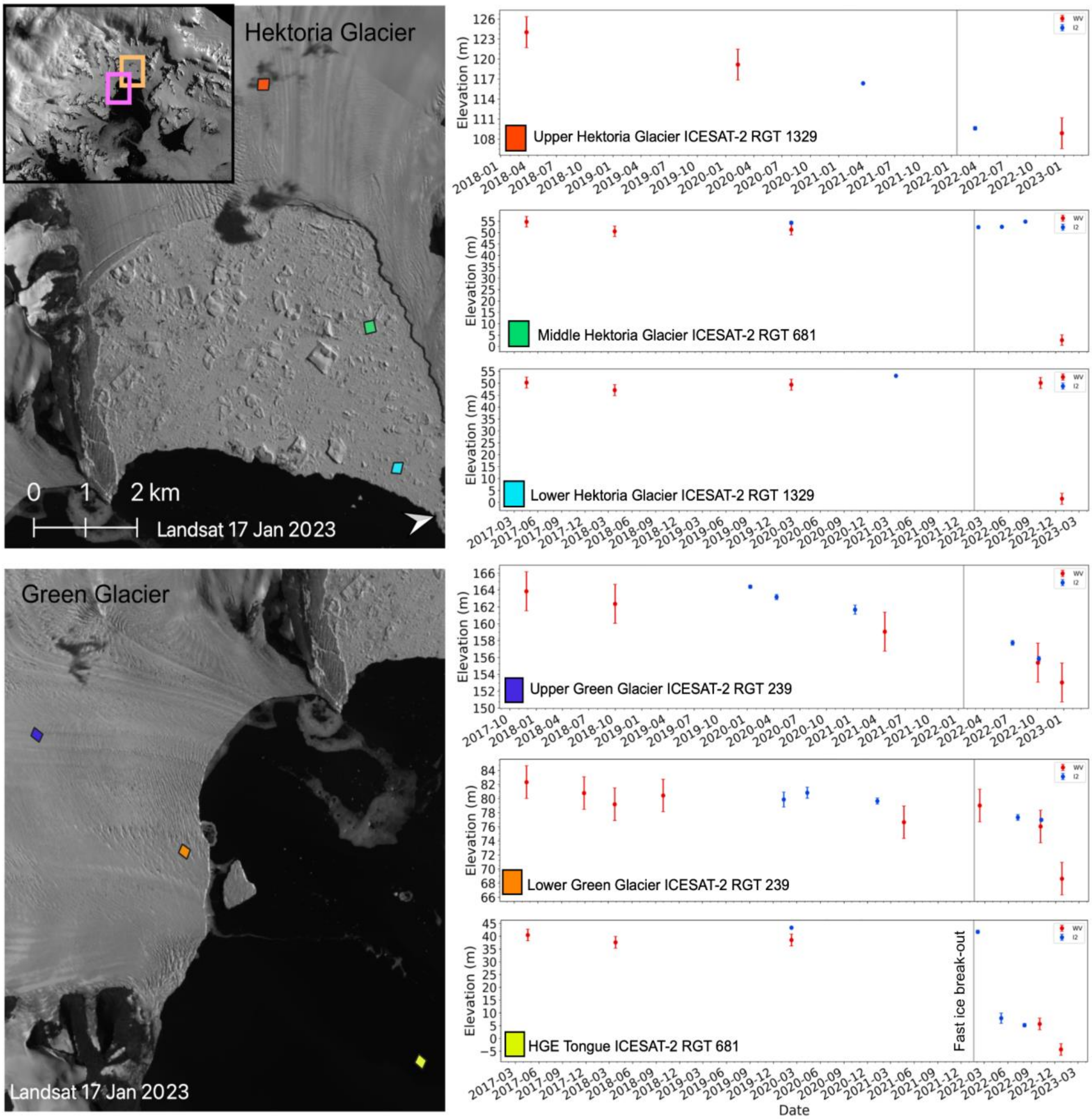

https://doi.org/10.5194/tc-2023-88
Preprint. Discussion started: 27 June 2023

Figure 11: Hektoria and Green Glacier system elevation changes through time. Background image is from 17 January 2023 Landsat. The pink box in the study area inset is the area depicted for Green Glacier and the orange box is Hektoria Glacier. The time series plot corresponds to the area of the box of the same color. The gray band indicates the date of the fast ice break-out event. Green Glacier points are the left panels and Hektoria Glacier points are the right panels.

5 Discussion

5.1 Synoptic scale climate patterns

The AP climate is subject to several different synoptic scale climate patterns. These patterns are drivers of the formation and demise of sea ice, fast ice, the mass balance and stability of the glaciers and ice shelves. Climate patterns and variability are driven by several modes with a variety of time scales, e.g., the Interdecadal Pacific Oscillation (IPO) at 10 to 30 years and SAM phase oscillations, changing on the scale of weeks to months. The IPO was in a negative phase from 2000 to 2014, favoring an increase of sea ice extent at ~$0.57 \pm 0.33 \times 10^6$ km^2 per decade (Meehl et al., 2016). Additionally, slightly cooler conditions around the AP in the 2010s limited the area of melt ponding on the Scar Inlet Ice Shelf and the northern Larsen C (Cape et al., 2015; Bevan et al., 2018). This situation may be broadly favorable for the formation of the Larsen B embayment fast ice, yet due to local variability it can be difficult to pinpoint its exact drivers in a specific season. It appears the IPO reversed in 2015/2016 but that remains to be confirmed (Li et al., 2021). The SAM index has been trending toward more frequent periods of positive phase for many decades (Kwon et al., 2020; Li et al., 2021). A positive SAM is generally associated with a deepening of the Amundsen Sea Low, which subsequently enhances northwesterly flow across the AP, bringing warm air masses and an increase in foehn events into this region (Turner et al., 2022; Li et al., 2021). A positive SAM is also correlated with AR events, due to enhanced moisture fluxes towards the Antarctic Peninsula and a more easterly storm track, which can increase warming on the lee side of the Antarctic Peninsula during AR-driven foehn events (Shields et al., 2022; Wille et al., 2021; Wille et al., 2022). Strong westerly winds increase sea ice drift eastward and northward, exposing the AP's eastern coast and ice fronts to open ocean. This may have caused the low sea ice cover in the Weddell Sea in summer 2021/2022 and low sea ice concentration in the corridor region in January 2022 (Turner et al., 2022).

We found that the climate of the Larsen B region was anomalously warm from November 2021 to January 2022. However, despite the climate being warmer, the number of melt days over the fast ice derived from the passive microwave data in this 2021/2022 season was not a record, and cumulative melt days in 2018/2019 and 2019/2022 significantly exceeded the total in 2021/2022 (Fig. 5). In 2021/2022, days with melt over 100% of the study area (i.e. all of the fast ice) were also lower than in any other season from 2013/2014 until 2020/2021. According to the optical imagery, melt ponds were evident in Landsat 8 satellite images mainly in November and December 2022. The areal extent of the melt ponds in the Larsen B region just prior to the fast ice break-out event in January 2022 was low (Fig. S4). These observations suggest that neither surface melting, nor

https://doi.org/10.5194/tc-2023-88
Preprint. Discussion started: 27 June 2023

The Cryosphere Discussions

related hydrofracturing of melt ponds, were a direct cause of the 19 January fast ice fracturing or the subsequent break-up, although they do point to a warmer fast ice cover at mid-summer of 2021/2022.

Antarctic sea ice extent and concentration reached a then-record low minimum in the satellite era in February 2022, ultimately leading to a sea-ice free corridor. The low sea ice concentration and westerly winds from a deep Amundsen Sea Low led to an open water corridor between the pack ice and the eastern side of the AP. As a result, the region in front of the Larsen B had the lowest total sea ice area since 2010 (Fig. 6). Therefore, for the first time since the formation of the persistent fast ice cover in 2011, a relatively ice-free corridor connected the fast ice front area to the open Southern Ocean. With low sea ice dampening, ocean swell events could impact the eastern fast ice and coastal areas in the summer for the first time in the preceding 11 years. These have been shown to destabilize fast ice and ice shelves (Banwell et al., 2017; Massom et al., 2018; Teder et al., 2022).

5.2 The fast ice break-out event

Despite high temperatures and surface melt and meltwater ponding (Scambos et al., 2003; Banwell et al., 2013), alongside thinning due to both basal melting and surface melting (Adusumili et al., 2018; Smith et al. 2020), known to be primary drivers of ice shelf collapse, our analysis shows that the Larsen B multi-year fast ice persisted through warm and high melt years (e.g., especially 2019-2020; Bevan et al 2020; Banwell et at., 2021) without breaking up. Until the 2021/2022 melt season, the absence of a sea ice-free corridor prevented large ocean swells from reaching the fast ice. Long period ocean swells, such that the wavelength is substantially greater than the ice thickness, can expose ice shelves and fast ice to flexural strains (Banwell et al., 2017; Massom et al., 2018). In our case, the fast ice was several meters thick, wave height was nearly 1.75 m, and the wave period at the time of the event was 5 to 6 s, corresponding to wavelengths of order of 40 m (Fig. 7). The resulting strains can weaken the outer margins of the ice through plate-bending and fracturing. As the outer margin breaks, the stress is redistributed within the fast ice, possibly initiating further fractures within the ice (Massom et al., 2018).

Once the fast ice fractured, it quickly drifted into the Weddell Sea; by 21 January the fast ice had drifted 9-16 km to the northeast out of the embayment. The rapid removal of the fast ice coincides with the presence of foehn winds that were likely caused by an AR event. Recently, ARs and AR-triggered foehn events have been linked to the collapse of ice shelves due to their ability to cause extreme surface melting and subsequent hydrofracture (Wille et al., 2022; Laffin et al., 2022). In this case, the foehn events caused by the AR were a factor. Here, we found that foehn events happened prior to, during, and after the January 2022 Larsen B wave event, potentially causing interior hydrofracturing, after the ocean swell fractured the outer margins of the fast ice, thereby redistributing the stress within the ice. Therefore, foehn events can be both a primary driver of ice break-up via hydrofracturing and a secondary driver via hastening the removal of floating ice, or, by creating corridors for wave entry to the ice fronts.

5.3 The initial glacier response

The presence of fast ice significantly affected the tributary glaciers' dynamics, providing significant backstress that permitted the tributary glaciers to readvance into the embayment during 2010 to 2022 after the initial break-up in 2002 (Fig. 2; Needell and Holschuh, 2023). The deceleration of the Scar Inlet Ice Shelf during the occupation of the multi-year fast ice indicates there was sufficient backstress to alter the ice shelf dynamics and likely the tributary glaciers as well, despite recent modelling results (Sun et al., in review). It is well known that rigid mélange and/or fast ice can allow tidewater glaciers or floating glacier tongues to advance (Moon et al., 2015; Gomez-Fell et al., 2022). Rigid mélange or fast ice have been observed and modelled to cease calving at glacier termini in Greenland and Antarctica (Robel et al., 2017; Cassotto et al., 2015; Banwell et al., 2017; Massom et al., 2010; Reeh et al., 2001). During the 2010 to 2022 period, Crane, Hektoria and Green readvanced and decelerated (Rott et al., 2018).

The calving regimes and dynamical changes of the Larsen B tributary glaciers are similar to their response after the 2002 Larsen B ice shelf disintegration, suggesting that calving is an immediate response to stress perturbations (Hulbe et al. 2008). For example, in the three years following the Larsen B ice shelf disintegration event (2002 to 2005), the Crane Glacier ice front and grounding zone retreated 18 km into the fjord, and the ice front height increased from 60 m to just over 100 m (Scambos et al., 2011, De Rydt et al., 2015). Simultaneously, the glacier trunk upstream of the ice front lost elevation at a rate of 35 m yr^{-1} (Shuman et al., 2011). Thus far, the 2022 event has caused Crane Glacier to retreat ~11 km in 14 months. However, significant thinning has yet to occur. Between 2002 and 2003, Crane Glacier ice flow increased rapidly, roughly 3-fold from ~500 m yr^{-1} to ~1500 m yr^{-1} (Rignot et al., 2004). Between 2022 to 2023 Crane Glacier ice flow speed increased from ~750 m yr^{-1} to 1050 m yr^{-1}. Crane Glacier has responded similarly to both losses of buttressing in the last 20 years, yet the magnitude of changes was greater in the immediate aftermath of the 2002 event. Hektoria's calving in 2022 is similar to the 2002 event where initially floating tabular bergs calved and then an arcuate calving front formed with large rifts and slumping. In 2022/2023, Hektoria retreated ~25 km, with ~10 km likely to be grounded ice, which is greater than the 2002 event in which Hektoria lost ~15 km of floating ice in the first year and it was not until two years after the loss of the ice shelf in 2004 that Hektoria began calving at its grounded terminus. This could possibly be explained with the lower Hektoria glacier being much closer to floatation in 2022 than it was in 2002. In that case, acceleration and thinning would have first been needed to bring the Hektoria Glacier to a height near floatation before significant retreat of grounded ice could occur after the 2022 event. In 2002 to 2003 Hektoria's ice flow speeds increased 8-fold from ~250 m yr^{-1} to over ~2000 m yr^{-1}. From 2022 to 2023 Hektoria's ice flow speeds increased from 300 m yr^{-1} to 1200 m yr^{-1} (Fig. 9). Although the magnitude is not as great as the 2002 event, an extreme acceleration has occurred. Hektoria's thinning from 2002 to 2003 was between 5 to 38 m yr^{-1} (Scambos et al., 2004), whereas the 2022 event resulted in thinning of between 8 to 11 m on Green Glacier from March 2022 to January 2023 (Fig. 11). Both Crane and Hektoria experienced rapid changes after both the 2002 and 2022 events. Comparison of the speeds, thinning, and retreat rates, reveals that the 2002 event had a greater impact on the glacier dynamics within the first year of the

https://doi.org/10.5194/tc-2023-88
Preprint. Discussion started: 27 June 2023

loss of ice shelf/multi-year fast ice buttressing. This is an expected response, as the loss of the Larsen B Ice Shelf should result in a higher debuttressing effect than the more recent loss of the much thinner fast ice.

6 Conclusions

The climate of the AP has been warming over the past several decades (Vaughan et al., 2003; Zagorodnov et al., 2012), interrupted by a decade-scale cooling that coincided with the formation of the fast ice in 2011 (Turner et al., 2016). During the 2021/2022 season the Larsen B region of the AP experienced anomalously high temperatures causing an ice-free corridor to open along the eastern coast of the peninsula that in turn allowed long period high amplitude swells to reach the fast ice. The sea ice concentration in the Weddell Sea in 2022 was the lowest in the satellite record (prior to 2023) and the sea ice area immediately near the Larsen B embayment was at its lowest since 2010.

The large-amplitude wave event with a long period swell that occurred 18 to 19 January reached the fast ice front via the ice-free corridor. We infer that this flexed the outer margin of the fast ice, causing it to fracture and redistribute the stresses within the thin ice plate, which would be seasonally at its weakest due to the recent warm air temperature. We note, however, that melt ponds and hydrofracture of the fast ice do not appear to play a direct role in this case. An AR and foehn wind event occurred during and after the fast ice break-out, contributing to the quick removal of the fast ice from the embayment.

All of the glacier responses following the Larsen B embayment fast ice break-out are reminiscent of the effects on glacier flow after the Larsen B ice shelf removal (i.e., extreme and varied), despite the fast ice being substantially thinner than the ice shelf (5 to 10 m compared to ~250 m). The fast ice was clearly buttressing the glaciers, and its removal led to obvious destabilization and dynamical changes. Several glaciers immediately began to lose their floating tongues in full-thickness tabular calving, and other glaciers experienced buoyancy-driven calving at their grounding zone. Over the following months several of the glaciers retreated rapidly into their fjords.

Antarctica’s coastline is fringed with multi-year fast ice that is likely buttressing large glaciers around the continent (Fraser et al., 2021). As the climate continues to change (Gilbert and Kittel, 2021), Antarctica's fast ice may be susceptible to breaking up due to exposure to new trigger mechanisms, such as previously dampened ocean swells. As Antarctic sea ice concentrations are projected to decrease over the current century (Holmes et al., 2022), this risk is inherently higher. Antarctic-wide fast ice buttressed glaciers are subject to substantial dynamical changes and potential retreat if the multi-year fast ice breaks up, similar to ice shelf tributary glaciers.

This case study affirms the importance of examining the impacts of synoptic-scale circulation patterns on foehn conditions, sea ice extent, and ocean swells on the Antarctic Peninsula. It is necessary not only to continue monitoring the glaciers in the

Larsen B area to fully understand their response to the loss of the fast ice, but to monitor other areas of Antarctica's coastline that may be susceptible to a similar fate.

Supplemental Information

Supplemental information can be found in tc-2023-88-supplement-version1.pdf.

Acknowledgements

We would like to thank Chris Shuman and Mark Fahnestock for their help in monitoring the break-out and suggesting processing tools. The British Antarctic Survey pilots who captured images of the initial fast ice break-up on 31 January 2022. The NSIDC for data availability and technical support. TAS and NEO received support from NASA award no. 80NSSC22K0386 and USGS award no. 140G0118. GPS data was collected using the LARISSA award NSF OPP 0732602 and NSF OPP 0732921. AFB received support from the U.S. National Science Foundation (NSF) under award no. 1841607.

Author Contributions:

NEO led the study, processed and analyzed the data, and wrote the manuscript. TAS initiated the idea and wrote the manuscript. GP processed the AMSR data to detect liquid water and AFB analyzed these data and produced Fig. 5. RSA, SM, and LM contributed to the plan of the research. MLM analyzed the AR events. JAS contributed to the climate analysis methods. MT and ECP processed and analyzed the GPS data. All authors contributed to the writing of the manuscript.

Competing interests:

The authors declare no conflict of interest.

Data Availability

Sea ice extent data is available on the University of Bremen sea ice webpage (https://seaice.uni-bremen.de/sea-ice-concentration/amsre-amsr2). Operation IceBridge data is available at NSIDC (https://nsidc.org/data/icebridge) as well as the ICESat-2 data (https://nsidc.org/data/atl06/versions/6). MODIS imagery can be viewed and downloaded on the Worldview interface (https://worldview.earthdata.nasa.gov). ERA-5 data are available at the Copernicus data store (https://cds.climate.copernicus.eu/cdsapp#!/home). WaveWatch III is available on CSIRO (https://data.csiro.au/collection/csiro:39819). The AMSR-E/2 data are available to download here: https://perscido.univ-grenoble-alpes.fr/datasets/DS391. The Reference Elevation Model of Antarctica is available via the Polar Geospatial Center

(Howat et al., 2022, https://www.pgc.umn.edu/data/rema/). The Worldview DEMs are available from Polar Geospatial Center upon request.

References

Adusumilli, S., Fricker, H. A., Siegfried,M. R., Padman, L., Paolo, F. S., and Ligtenberg, S. R. M.:. Variable basal melt rates of Antarctic Peninsula ice shelves, 1994–2016. Geophys. Res. Lett., 45, 4086–4095. doi:10.1002/2017GL076652, 2018.

Amundson, J. M., Fahnestock, M., Truffer, M., Brown, J., Lüthi, M. P., and Motyka, R. J.: Ice mélange dynamics and implications for terminus stability, Jakobshavn Isbræ, Greenland, J. Geophys. Res., 115, F01005, doi:10.1029/2009JF001405, 2010.

Banwell, A. F., MacAyeal, D. R., and Sergienko, O. V.: Breakup of the Larsen B Ice Shelf triggered by chain reaction drainage of supraglacial lakes, Geophys. Res. Lett., 40, 5872– 5876, doi:10.1002/2013GL057694, 2013.

Banwell, A. F. and Macayeal, D. R.: Ice-shelf fracture due to viscoelastic flexure stress induced by fill/drain cycles of supraglacial lakes, Antarct. Sci., 27(6), 587-597, doi:10.1017/S0954102015000292, 2015.

Banwell, A. F., Willis, I. C., Goodsell, B., Macdonald, G. J., Mayer, D., Powell, A. and MacAyeal, D. R.: Calving and Rifting on McMurdo Ice Shelf, Antarctica, Ann. Glaciol., 58(75pt1), 78-87, doi:10.1017/aog.2017.12, 2017.

Banwell, A. F., Datta, R. T., Dell, R. L., Moussavi, M., Brucker, L., Picard, G., Shuman, C. A., and Stevens, L. A.: The 32-year record-high surface melt in 2019/2020 on the northern George VI Ice Shelf, Antarctic Peninsula, Cryosphere, 15, 909–925, doi:10.5194/tc-15-909-2021, 2021.

Banwell, A.F., Wever, N., Dunmire, D., and Picard, G.: Quantifying Antarctic-wide ice-shelf surface melt volume using microwave and firn model data: 1980 to 2021, Geophys. Res. Lett., doi:10.1029/2023GL102744, 2023.

Bassis, J. N., Berg, B., Crawford, A. J., and Benn, D. I.: Transition to marine ice cliff instability controlled by ice thickness gradients and velocity, Science, 372(6548), 1342– 1344. doi:10.1126/science.abf6271, 2021.

Benn, D. I., Åström, J., Zwinger, T., Todd, J., Nick, F. M., Cook, S., Hulton, N. R. and Luckman, A.: Melt-under-cutting and buoyancy-driven calving from tidewater glaciers: New insights from discrete element and continuum model simulations, J. Glaciol., 63(240), 691-702. doi:10.1017/jog.2017.41, 2017.

Berthier, E., Scambos, T. A., and Shuman, C. A.: Mass loss of Larsen B tributary glaciers (Antarctic Peninsula) unabated since 2002, Geophys. Res. Lett., 39(13), 1–6. doi:10.1029/2012GL051755, 2012.

Bevan, S. L., Luckman, A. J., Kuipers Munneke, P., Hubbard, B., Kulessa, B., and Ashmore, D. W.: Decline in surface melt duration on Larsen C Ice Shelf revealed by the advanced scatterometer (ASCAT), Earth Space Sci., 5, 578–591. doi:10.1029/2018EA000421, 2018.

Borstad, C. P., Rignot, E., Mouginot, J. and Schodlok, M. P.: Creep deformation and buttressing capacity of damaged ice shelves: theory and application to Larsen C ice shelf, Cryosphere, 7(6), 1931-1947, doi:10.5194/tc-7-1931-2013, 2013.

Bozkurt, D., Rondanelli, R., Marin, J. C., and Garreaud, R.L: Foehn event triggered by an atmospheric river underlies record-setting temperature along continental Antarctica, J. Geophys. Res. Atmos, 123, 3871–3892. doi:10.1002/2017JD027796, 2018.

Cape, M. R., Vernet, M., Skvarca, P., Marinsek, S., Scambos, T. and Domack, E.: Foehn winds link climate-driven warming to ice shelf evolution in Antarctica, J. Geophys. Res. Atmos, 120(21), 11-037, doi:10.1002/2015JD023465, 2015.

Carrasco, J. F., Bozkurt, D., and Cordero, R.: A review of the observed air temperature in the Antarctic Peninsula. Did the warming trend come back after the early 21st hiatus?, Polar Sci., 28, 100653. doi: 0.1016/j.polar.2021.100653, 2021.

Cassotto, R., Fahnestock, M., Amundson, J., Truffer, M., and Joughin, I.:. Seasonal and interannual variations in ice melange and its impact on terminus stability, Jakobshavn Isbræ, Greenland, J. Glaciol., 61(225), 76-88. doi:10.3189/2015JoG13J235, 2015.

Cook, A. J. and Vaughan, D. G.: Overview of areal changes of the ice shelves on the Antarctic Peninsula over the past 50 years, Cryosphere, 4(1), 77-98, doi:10.5194/tc-4-77-2010, 2010.

Datta, R. T., Tedesco, M., Fettweis, X., Agosta, C., Lhermitte, S., Lenaerts, J. T. M., and Wever, N.: The effect of Foehn-induced surface melt on firn evolution over the northeast Antarctic peninsula, Geophys. Res. Lett., 46, 3822– 3831, doi:10.1029/2018GL080845, 2019.

Doake, C., and Vaughan, D.: Rapid disintegration of the Wordie Ice Shelf in response to atmospheric warming, Nature, 350, 328–330, doi:10.1038/350328a0, 1991.

Fahnestock, M., Scambos, T., Moon, T., Gardner, A., Haran, T., and Klinger, M.: Rapid large-area mapping of ice flow using Landsat 8, Remote Sens Environ, 185, 84-94. doi:10.1016/j.rse.2015.11.023, 2016.

Fogt, R. L., and Marshall, G. J.: The Southern Annular Mode: Variability, trends, and climate impacts across the Southern Hemisphere. Rev. Clim. Change, 11(4), 1–24. doi:10.1002/wcc.652, 2020.

Fox, C., and Squire, V. A.: Coupling between the ocean and an ice shelf. Ann. Glaciol., *15*, 101-108, doi:10.3189/1991AoG15-1-101-108, 1991.

Fraser, A. D., Massom, R. A., Handcock, M. S., Reid, P., Ohshima, K. I., Raphael, M. N., Cartwright, J., Klekociuk, A. R., Wang, Z., and Porter-Smith, R.: Eighteen-year record of circum-Antarctic landfast-sea-ice distribution allows detailed baseline characterisation and reveals trends and variability, Cryosphere, 15, 5061–5077, doi:10.5194/tc-15-5061-2021, 2021.

Gardner, A. S., Moholdt, G., Scambos, T., Fahnstock, M., Ligtenberg, S., Broeke, M.V.D. and Nilsson, J.: Increased West Antarctic and unchanged East Antarctic ice discharge over the last 7 years. Cryosphere, 12(2), 521-547. doi:10.5194/tc-12-521-2018, 2018.

Gilbert, E., and Kittel, C.: Surface melt and runoff on Antarctic ice shelves at 1.5°C, 2°C, and 4°C of future warming. Geophys. Res. Lett., 48, e2020GL091733, https://doi.org/10.1029/2020GL091733, 2021.

Glasser, N. F. and Scambos, T. A.: A structural glaciological analysis of the 2002 Larsen B ice-shelf collapse, J. Glaciol., 54(184), 3-16, doi:10.3189/002214308784409017, 2008.

Glasser, N. F., Scambos, T. A., Bohlander, J., Truffer, M., Pettit, E., and Davies, B. J.: From ice-shelf tributary to tidewater glacier: continued rapid recession, acceleration and thinning of Röhss Glacier following the 1995 collapse of the Prince Gustav Ice Shelf, Antarctic Peninsula. J. Glaciol., 57(203), 397–406, doi:10.3189/002214311796905578, 2011.

Gomez-Fell, R., Rack, W., Purdie, H., and Marsh, O.: Parker Ice Tongue collapse, Antarctica, triggered by loss of stabilizing land-fast sea ice. Geophys. Res. Lett., 49, e2021GL096156. doi:10.1029/2021GL096156, 2022.

Holmes, C. R., Bracegirdle, T. J., and Holland, P. R.: Antarctic sea ice projections constrained by historical ice cover and future global temperature change. Geophys. Res. Lett., 49, e2021GL097413. doi:10.1029/2021GL097413, 2022.

Howat, I., Porter C., Noh, M-J., Erik, H., Samuel, K., Danish, E., Tomko, K., Gardiner, J., Negrete, A., Yadav, B., Klassen, J., Kelleher, C., Cloutier, M., Bakker, J., Enos, J., Arnold, G., Bauer, G., Morin, P.: The Reference Elevation Model of Antarctica - Strips, Version 4.1, Harvard Dataverse, V1, doi:10.7910/DVN/X7NDNY, 2022.

Hulbe, C. L., Scambos, T. A., Youngberg, T. and Lamb, A.K.: Patterns of glacier response to disintegration of the Larsen B ice shelf, Antarctic Peninsula. Glob Planet Change, 63(1), 1-8, doi:10.1016/j.gloplacha.2008.04.001, 2008.

Jeffries, M. O.: Arctic ice shelves and ice islands: origin, growth and disintegration, physical characteristics, structural-stratigraphic variability, and dynamics. Rev. Geophys. 30(3), 245–267. doi:10.1029/92RG00956, 1992.

Khazendar, A., Rignot, E. and Larour, E.: Larsen B Ice Shelf rheology preceding its disintegration inferred by a control method. Geophys. Res. Lett., 34(19), doi:10.1029/2007GL030980, 2007.

King, J. C., Turner, J., Marshall, G. J., Connolley, W. M. and Lachlan-Cope, T .A.: Antarctic Peninsula climate variability and its causes as revealed by analysis of instrumental records. Antarct. Res. Ser., 79, 17-30, doi:10.1029/AR079p0017, 2003.

Laffin, M. K., Zender, C. S., van Wessem, M., and Marinsek, S.: The role of föhn winds in eastern Antarctic Peninsula rapid ice shelf collapse, Cryosphere, 16, 1369–1381, doi:10.5194/tc-16-1369-2022, 2022.

Leeson, A. A., Van Wessem, J. M., Ligtenberg, S. R. M., Shepherd, A., Van Den Broeke, M. R., Killick, R., ... and Colwell, S.: Regional climate of the Larsen B embayment 1980-2014. J. Glaciol., 63(240), 683–690. https://doi.org/10.1017/jog.2017.39, 2017.

Lei, Y., Gardner, A. and Agram, P.: Autonomous Repeat Image Feature Tracking (autoRIFT) and Its Application for Tracking Ice Displacement. Remote Sens, 13(4), 749. doi:10.3390/rs13040749, 2021.

Li, X., Cai, W., Meehl, G. A., Chen, D., Yuan, X., Raphael, M., ... and Song, C.: Tropical teleconnection impacts on Antarctic climate changes, Nat Rev Earth Environ, 2(10), 680–698. doi:10.1038/s43017-021-00204-5, 2021.

Liang, K., Wang, J., Luo, H., and Yang, Q.: The role of atmospheric rivers in Antarctic sea ice variations. Geophys. Res. Lett., 50, e2022GL102588. https://doi.org/10.1029/2022GL102588, 2023.

van Lipzig, N. P. M., Marshall, G. J., Orr, A., and King, J. C.: The Relationship between the Southern Hemisphere Annular Mode and Antarctic Peninsula Summer Temperatures: Analysis of a High-Resolution Model Climatology. J. Climate, 21, 1649–1668, doi:10.1175/2007JCLI1695.1, 2008

Marshall, G. J., Orr, A., van Lipzig, N. P., and King, J. C.: The Impact of a Changing Southern Hemisphere Annular Mode on Antarctic Peninsula Summer Temperatures. J. Climate, 19, 5388–5404, doi:10.1175/JCLI3844.1, 2006.

Massom, R. A., Giles, A. B., Fricker, H. A., Warner, R. C., Legrésy, B., Hyland, G., Young, N., and Fraser, A. D : Examining the interaction between multi-year fast ice and the Mertz Glacier Tongue, East Antarctica: Another factor in ice sheet stability?, J. Geophys. Res., 115, C12027, doi:10.1029/2009JC006083, 2010.

Massom, R. A., Scambos, T. A., Bennetts, L. G., Reid, P., Squire, V. A., and Stammerjohn, S. E.: Antarctic ice shelf disintegration triggered by sea ice loss and ocean swell, Nature, 558.7710, 383-389, doi:10.1038/s41586-018-0212-1 2018.

Meehl, G. A., Arblaster, J. M., Bitz, C. M., Chung, C. T. & Teng, H.: Antarctic sea- ice expansion between 2000 and 2014 driven by tropical Pacific decadal climate variability. Nat. Geosci. 9, 590–595, doi:10.1038/ngeo2751, 2016.

Meier, W. N., T. Markus, and J. C. Comiso.: AMSR-E/AMSR2 Unified L3 Daily 12.5 km Brightness Temperatures, Sea Ice Concentration, Motion & Snow Depth Polar Grids, Version 1. Boulder, Colorado USA. NASA National Snow and Ice Data Center Distributed, Active Archive Center. Accessed May 2022. doi:10.5067/RA1MIJOYPK3P, 2018.

Melton, S., Alley, R., Anandakrishnan, S., Parizek, B., Shahin, M., Stearns, L., . . . Finnegan, D.: Meltwater drainage and iceberg calving observed in high-spatiotemporal resolution at Helheim Glacier, Greenland. J. Glaciol., 68(270), 812-828, doi:10.1017/jog.2021.141, 2022.

Mercer, J. H.: West Antarctic ice sheet and CO2 greenhouse effect: a threat of disaster, Nature, 271, 321–325, https://doi.org/10.1038/271321a0, 1978.

Moon, T., Joughin, I., and Smith, B.: Seasonal to multiyear variability of glacier surface velocity, terminus position, and sea ice/ice mélange in northwest Greenland, J. Geophys. Res. Earth Surf., 120, 818– 833. doi: 10.1002/2015JF003494, 2015.

Murray, T., Selmes, N., James, T. D., Edwards, S., Martin, I., O'Farrell, T., Aspey, R., Rutt, I., Nettles, M., and Baugé, T.: Dynamics of glacier calving at the ungrounded margin of Helheim Glacier, southeast Greenland. J. Geophys. Res. Earth Surf., 120, 964–982. doi:10.1002/2015JF003531, 2015

Murty, T. S.: Modification of hydrographic characteristics, tides, and normial modes by ice cover. Mar. Geod., 9(4), 451-468. doi:10.1080/15210608509379538, 1985.

Needell, C., and Holschuh, N.: Evaluating the retreat, arrest, and regrowth of Crane Glacier against marine ice cliff process models. Geophys. Res. Lett., 50, e2022GL102400. https://doi.org/10.1029/2022GL102400, 2023.

Orr, A., Marshall, G. J., Hunt, J. C. R., Sommeria, J., Wang, C., van Lipzig, N. P. M., Cresswell, D., and King, J. C.: Characteristics of Summer Airflow over the Antarctic Peninsula in Response to Recent Strengthening of Westerly Circumpolar Winds. J. Atmos. Sci., 65, 1396–1413, https://doi.org/10.1175/2007JAS2498.1, 2008.

Parizek, B. R., Christianson, K., Alley, R. B., Voytenko, D., Vaňková, I., Dixon, T. H., ... and Holland, D. M.: Ice-cliff failure via retrogressive slumping, Geology, 47(5):449-452, doi:10.1130/G45880.1, 2019.

Picard, G., Fily, M., and Gallee, H., 2007. Surface melting derived from microwave radiometers: A climatic indicator in Antarctica. Ann. Glaciol., 46, 29-34. doi:10.3189/172756407782871684

Picard, G., Leduc-Leballeur, M., Banwell, A. F., Brucker, L., and Macelloni, G.: The sensitivity of satellite microwave observations to liquid water in the Antarctic snowpack, Cryosphere, 16, 5061–5083, doi:10.5194/tc-16-5061-2022, 2022.

Reeh, N., Thomsen, H., Higgins, A., and Weidick, A.: Sea ice and the stability of north and northeast Greenland floating glaciers. Ann. Glaciol., 33, 474-480. doi:10.3189/172756401781818554, 2001.

Rignot, E., Casassa, G., Gogineni, P., Krabill, W., Rivera, A., and Thomas, R.: Accelerated ice discharge from the Antarctic Peninsula following the collapse of Larsen B ice shelf, Geophys. Res. Lett., 31, L18401, doi:10.1029/2004GL020697, 2004.

Robinson, W. H. and Haskell, T. G.: Travelling flexural waves in the Erebus Glacier Tongue, McMurdo Sound, Antarctica, Cold Reg Sci Technol, 20.3, 289-293, doi:10.1016/0165-232X(92)90035-S, 1992.

Rott, H., Skvarca, P. and Nagler, T.: Rapid collapse of northern Larsen ice shelf, Antarct. Sci., 271(5250), 788-792, doi:10.1126/science.271.5250.788, 1996.

Rott, H., Rack, W., Nagler, T. and Skvarca, P.: Climatically induced retreat and collapse of northern Larsen Ice Shelf, Antarctic Peninsula, Ann. Glaciol., 27, 86-92, doi:10.3189/S0260305500017262, 1998.

Rott, H., Abdel Jaber, W., Wuite, J., Scheiblauer, S., Floricioiu, D., Van Wessem, J. M., Nagler, T., Miranda, N., and Van Den Broeke, M. R.: Changing pattern of ice flow and mass balance for glaciers discharging into the Larsen A and B embayments, Antarctic Peninsula, 2011 to 2016, Cryosphere, 12(4), 1273–1291. doi:10.5194/tc-12-1273-2018, 2018.

De Rydt J., Gudmundsson G. H., Rott H., and Bamber J. L.: Modeling the instantaneous response of glaciers after the collapse of the Larsen B Ice Shelf, Geophys. Res. Lett., 42(13):5355-5363, 2015.

Scambos, T., Hulbe, C., and Fahnestock, M.: Climate-induced ice shelf disintegration in the Antarctic Peninsula, in: Antarctic Peninsula Climate Variability: Historical and Paleoenvironmental Perspectives. Antarctic Research Series, 79, edited by: Domack, E., Leventer, A., Burnett, A., Bindschadler, R., Convey, P., and Kirby, M., AGU, Washington, DC, 79–92, doi:10.1029/AR079p0079, 2003.

Scambos, T. A., Bohlander, J. A., Shuman, C. A., and Skvarca, P.: Glacier acceleration and thinning after ice shelf collapse in the Larsen B embayment, Antarctica, Geophys. Res. Lett., 31, L18402, doi:10.1029/2004GL020670, 2004.

Scambos, T., R. Ross, R. Bauer, Y. Yermolin, P. Skvarca, D. Long, J. Bohlander, and T. Haran.: Calving and ice-shelf break-up processes investigated by proxy: Antarctic tabular iceberg evolution during northward drift, J. Glaciol,, 54(187), 579-591. doi:10.3189/002214308786570836, 2008.

Scambos, T., Fricker, H. A., Liu, C. C., Bohlander, J., Fastook, J., Sargent, A., Massom, R. and Wu, A. M.: Ice shelf disintegration by plate bending and hydro-fracture: Satellite observations and model results of the 2008 Wilkins ice shelf break-ups. Earth Planet. Sci. Lett., 280(1-4), 51-60. doi:10.1016/j.epsl.2008.12.027, 2009.

Scambos, T.A., Ross, R., Haran, T., Bauer, R., Ainley, D.G., Seo, K.W., De Keyser, M., Behar, A. and MacAyeal, D.R.: A camera and multisensor automated station design for polar physical and biological systems monitoring: AMIGOS. J. Glaciol., 59(214). doi:10.3189/2013JoG12J170. 2013.

Scambos, T., Moussavi, M. S., Abdalati, W. and Pettit, E. C.: December. Evolution of fast ice thickness from Cryosat-2 radar altimetry data, a case study in Scar Inlet, Antarctica. AGU Fall Meeting Abstracts (Vol. 2017, pp. C21G-1181), 2017.

https://doi.org/10.5194/tc-2023-88
Preprint. Discussion started: 27 June 2023

Shields, C. A., Wille, J. D., Marquardt Collow, A. B., Maclennan, M., and Gorodetskaya, I. V.: Evaluating uncertainty and modes of variability for Antarctic atmospheric rivers. Geophys. Res. Lett., 49, e2022GL099577. doi:10.1029/2022GL099577, 2022.

Shuman C. A., Berthier E., and Scambos T. A.: 2001-2009 Elevation and mass losses in the Larsen A and B embayments, Antarctic Peninsula, J. Glaciol., 57(204):737-754. doi:10.3189/002214311797409811, 2011.

Shuman, C., Scambos, T. and Berthier, E.: Ice loss processes in the Seal Nunataks ice shelf region from satellite altimetry and imagery. Ann. Glaciol, 57(73), 94-104, doi:10.1017/aog.2016.29, 2016.

Skvarca, P., Rack, W., Rott, H. and Donángelo, T. I.: Climatic trend and the retreat and disintegration of ice shelves on the Antarctic Peninsula: an overview, Polar Res, 18(2), 151-157, doi:10.1111/j.1751-8369.1999.tb00287, 1999.

Smith, B., S. Adusumilli, B. M. Csathó, D. Felikson, H. A. Fricker, A. Gardner, N. Holschuh, J. Lee, J. Nilsson, F. S. Paolo, M. R. Siegfried, T. Sutterley, and the ICESat-2 Science Team: ATLAS/ICESat-2 L3A Land Ice Height, Version 5,. Boulder, Colorado USA. NASA National Snow and Ice Data Center Distributed Active Archive Center. doi:10.5067/ATLAS/ATL06.005. Date Accessed 09-12-2022, 2021.

Spreen, G., Kaleschke, L., and Heygster, G.: Sea ice remote sensing using AMSR-E 89 GHz channels, J. Geophys. Res., 113, C02S03, doi:10.1029/2005JC003384, 2008.

Sun, Y., Riel, B., Minchew, B.: Disintegration and Buttressing Effect of the Landfast Sea Ice in the Larsen B Embayment, Antarctic Peninsula. ESS Open Archive, doi:10.22541/essoar.168167149.94349869/v1, preprint April 2023,

Teder, N. J., Bennetts, L. G., Reid, P. A., and Massom, R. A.: Sea ice-free corridors for large swell to reach Antarctic ice shelves. Environ. Res. Lett., 17(4), 045026, doi:10.1088/1748-9326/ac5edd, 2022.

Torinesi, O., Fily, M., and Genthon, C.: Variability and Trends of the Summer Melt Period of Antarctic Ice Margins since 1980 from Microwave Sensors. J. Climate, 16, 1047–1060, doi:10.1175/1520-0442(2003)016<1047:VATOTS>2.0.CO;2, 2003.

Turner, J., Lu, H., White, I., King, J. C., Phillips, T., Hosking, J. S., Bracegirdle, T. J., Marshall, G. J., Mulvaney, R. and Deb, P.: Absence of 21st century warming on Antarctic Peninsula consistent with natural variability, Nature, 535, 411–415. doi:10.1038/nature18645, 2016.

https://doi.org/10.5194/tc-2023-88
Preprint. Discussion started: 27 June 2023

The Cryosphere Discussions
Open Access

Turner, J., Holmes, C., Caton Harrison, T., Phillips, T., Jena, B., Reeves-Francois, T., et al.: Record low Antarctic sea ice cover in February 2022. Geophys. Res. Lett., 49, e2022GL098904. doi:10.1029/2022GL098904, 2022.

Van Wessem, J. M., Reijmer, C. H., Van De Berg, W. J., van Den Broeke, M. R., Cook, A. J., Van Ulft, L. H. and Van Meijgaard, E.: Temperature and wind climate of the Antarctic Peninsula as simulated by a high-resolution Regional Atmospheric Climate Model. J. Clim., 28(18), 7306–7326. doi:10.1175/JCLI-D-15-0060.1, 2015.

Wellner, J.S., Scambos, T., Domack, E.W., Vernet, M., Leventer, A., Balco, G., Brachfeld, S., Cape, M.R., Huber, B., Ishman, S. and McCormick, M.L.: The Larsen ice shelf system, Antarctica (LARISSA): Polar systems bound together, changing fast. GSA Today, 29(8). doi:10.1130/GSATG382A.1, 2019

White, A., Copland, L., Mueller, D., and Van Wychen, W.: Assessment of historical changes (1959-2012) and the causes of recent break-ups of the Petersen ice shelf, Nunavut, Canada. Ann. Glaciol., 56(69), 65-76. doi:10.3189/2015AoG69A687, 2015.

Wille, J. D., Favier, V., Dufour, A., Gorodetskaya, I. V., Turner, J., Agosta, C., and Codron, F.: West Antarctic surface melt triggered by atmospheric rivers. Nat. Geosci. 12, 911–916, https://doi.org/10.1038/s41561-019-0460-1, 2019.

Wille, J. D., Favier, V., Gorodetskaya, I. V., Agosta, C., Kittel, C., Beeman, J. C., Jourdain, N. C., Lenaerts, J. T. M., and Codron, F.: Antarctic atmospheric river climatology and precipitation impacts. J. Geophys. Atmos., 126, e2020JD033788. doi:10.1029/2020JD033788, 2021.

Wille, J. D., Favier, V., Jourdain, N. C., Kittel, C., Turton, J. V., Agosta, C., ... and Berchet, A.: Intense atmospheric rivers can weaken ice shelf stability at the Antarctic Peninsula. Nat. Commun Earth & Environ, 3(1), doi:10.1038/s43247-022-00422-9, 2022.

Young, N., Turner, D., Hyland, G., and Williams, R.: Near-coastal iceberg distributions in East Antarctica, 50-145° E. Ann. Glaciol, 27, 68-74. doi:10.3189/1998AoG27-1-68-74, 1998.

Zagorodnov, V., Nagornov, O., Scambos, T.A., Muto, A., Mosley-Thompson, E., Pettit, E.C. and Tyuflin, S.: Borehole temperatures reveal details of 20th century warming at Bruce Plateau, Antarctic Peninsula. Cryosphere, 6(3), 675-686, doi: 10.5194/tc-6-675-2012, 2012.